

TECHNICAL UNIVERSITY OF CRETE  
School of Production Engineering & Management



M.Sc. Dissertation

---

**Methodology development for strength analysis of a  
Diffuser Augmented Wind Turbine (DAWT)**

---

Michael Georgiou

Supervisor: Prof. I.K. Nikolos

Chania, July 2022



The present thesis is approved by the following jury:

**Thesis Examination Committee:**

---

**Dr. Ioannis K. Nikolos (Supervisor)**

Professor, School of Production Engineering and Management,  
Technical University of Crete, Chania, Greece

**Dr. Anargiros Delis**

Associate Professor, School of Production Engineering and Management,  
Technical University of Crete, Chania, Greece

**Dr. George Arampatzis**

Assistant Professor, School of Production Engineering and Management,  
Technical University of Crete, Chania, Greece



# Abstract

M.Sc. Dissertation

## **Methodology development for strength analysis of a Diffuser Augmented Wind Turbine (DAWT)**

by Michael GEORGIOU

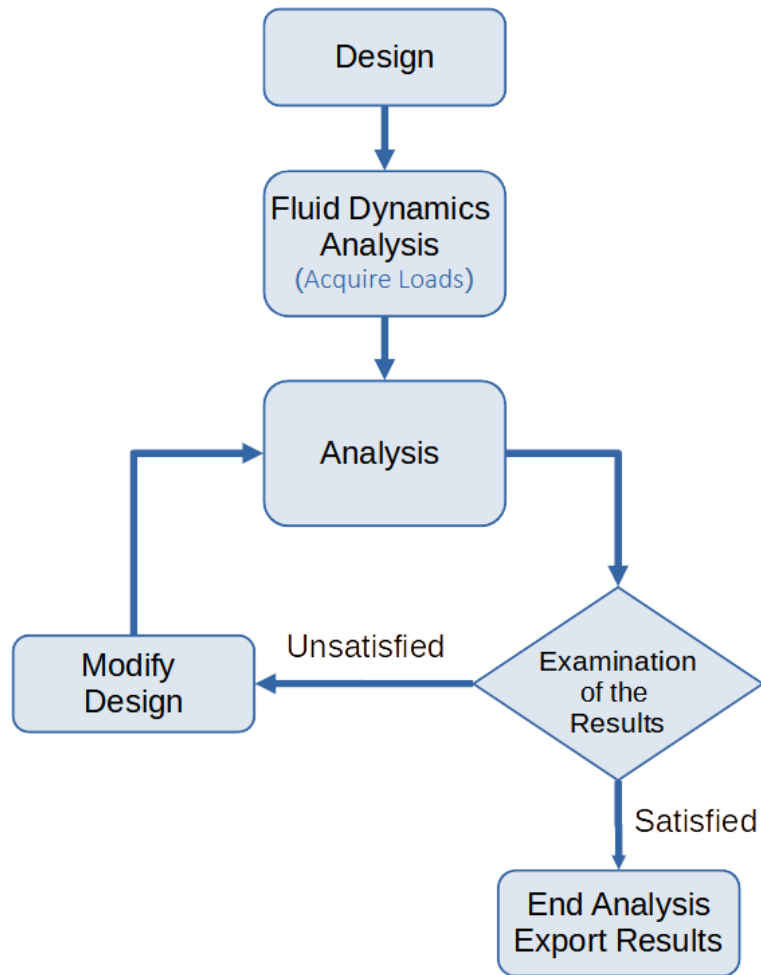
In the present work, we have studied the structural stability of the inner column of a Diffuser Augmented Wind Turbine (DAWT). The study model is an existing, under-development wind turbine.

Diffuser Augmented Wind Turbines function extremely well in terms of performance. The volume of the diffuser causes the ambient air to redirect and accelerate as it passes through the tunnel in the center of the diffuser. This additional flow and acceleration provide a higher energy output. Increasing to larger diameters this advantage reversing and turning it into a greater stumbling block. The wind resistance that augments the energy output is carried through the structure to the ground. This also increases the forces that the structure must withstand to tremendous levels. Unfortunately, this stumbling block limits the size of DAWTs; therefore they cannot directly compete with Horizontal Axis Wind Turbines (HAWT), whose development has taken them to unfathomable heights.

This does not mean that there is no reason for further research and development of DAWTs, which, as we have already mentioned, have significantly higher performance at similar blade diameters compared to HAWTs. DAWTs may be an alternative in many specific locations and may be a solution that is worth investigating in the fight against climate change.

As our study shows, the DAWT's structure is subjected to very strong frontal forces, due to the drag of the diffuser. For this reason, we intend to investigate the strength of the metal column holding the diffuser, using finite element analysis (FEA). We have attempted to strengthen the critical points while keeping the overall size narrow. We are trying to find a technically and economically feasible solution to the problem and have tried to optimize the project to some extent. The whole process is illustrated in the following diagram. This cycle was performed a

number of times, while in this study we present only the final iteration and the corresponding results.



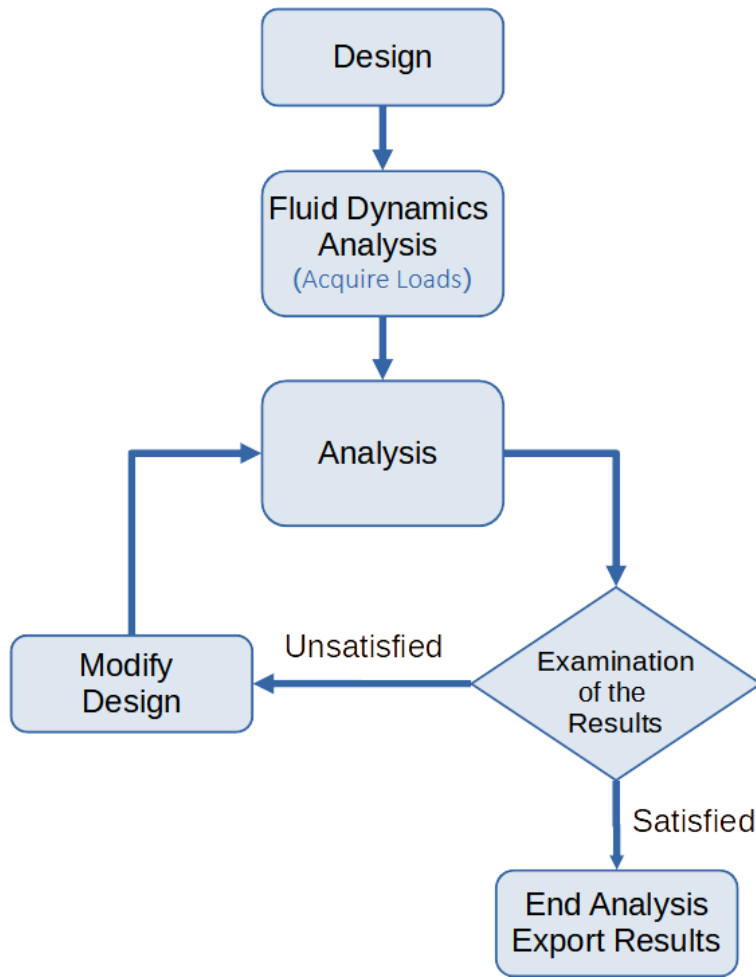
# Περίληψη

Στην παρούσα εργασία έχουμε μελετήσει την στατικότητα της εσωτερικής κολόνας μιας ανεμογεννήτριας εφοδιασμένης με διαχύτη. Πρόκειται για μια υπό ανάπτυξη πρότυπης ανεμογεννήτριας με προοπτική την εμπορική της υλοποίηση.

Οι ανεμογεννήτριες με διαχύτη λειτουργούν εξαιρετικά καλά, όσον αφορά στην απόδοση. Ο όγκος του διαχύτη προκαλεί την ανακατεύθυνση και επιτάχυνση του περιβάλλοντος αέρα, καθώς αυτός διέρχεται μέσα από τη δίοδο στο κέντρο του διαχύτη. Αυτή η πρόσθετη ροή και η επιτάχυνση παρέχουν υψηλότερη ενεργειακή απόδοση. Με την ανάπτυξη σε μεγαλύτερες διαμέτρους αυτό το πλεονέκτημα αντιστρέφεται και μετατρέπεται σε σημαντικό εμπόδιο. Η αντίσταση του ανέμου (που επιφέρει την αύξηση στην παραγωγής ενέργειας) μεταφέρεται μέσω της κατασκευής στο έδαφος. Αυτό αυξάνει επίσης τις δυνάμεις που πρέπει να αντέξει η κατασκευή σε τρομακτικά επίπεδα. Δυστυχώς, αυτό το εμπόδιο περιορίζει το μέγεθος των DAWT - ως εκ τούτου, δεν μπορούν να ανταγωνιστούν άμεσα τις ανεμογεννήτριες οριζόντιου άξονα (HAWT), η ανάπτυξη των οποίων τις έχει οδηγήσει σε δυσθεώρητα ύψη.

Αυτό δεν σημαίνει ότι δεν υπάρχει λόγος για περαιτέρω έρευνα και ανάπτυξη των DAWT, οι οποίες, όπως έχουμε ήδη αναφέρει, έχουν σημαντικά υψηλότερη απόδοση σε παρόμοιες διαμέτρους πτερυγίων σε σύγκριση με τις HAWT. Οι DAWT μπορεί να αποτελέσουν μια εναλλακτική λύση σε ορισμένες περιπτώσεις και μπορεί να αποτελέσουν μια λύση που αξίζει να διερευνηθεί στον αγώνα κατά της κλιματικής αλλαγής.

Όπως δείχνει και η παρούσα μελέτη, η δομή της DAWT υπόκειται σε πολύ ισχυρές μετωπικές δυνάμεις, λόγω της αντίστασης του διαχύτη. Για το λόγο αυτό, σκοπεύουμε να διερευνήσουμε την στατική αντοχή της μεταλλικής κολόνας που συγκρατεί το διαχύτη, χρησιμοποιώντας ανάλυση πεπερασμένων στοιχείων (FEA). Προσπαθήσαμε να ενισχύσουμε τα κρίσιμα σημεία, διατηρώντας παράλληλα το συνολικό μέγεθος μικρό. Προσπαθούμε να βρούμε μια τεχνικά και οικονομικά εφικτή λύση στο πρόβλημα και έχουμε προσπαθήσει να βελτιστοποιήσουμε το έργο σε κάποιο βαθμό. Η όλη διαδικασία απεικονίζεται στο ακόλουθο διάγραμμα. Ο κύκλος αυτός εκτελέστηκε αρκετές φορές, ενώ στην παρούσα μελέτη παρουσιάζουμε μόνο την τελική επανάληψη και τα αντίστοιχα αποτελέσματα.



# Acknowledgements

It's my pleasant duty to express my sincere regards and grateful obligation to all those who have contributed to the accomplishment of my research work.

Above all, I would like to thank Professor I.K. Nikolos for everything he taught me during my studies. The trust and support he has given me during our long collaboration have been invaluable.

In addition, I would like to thank my laboratory colleague Mr. Stavros Leloudas for his invaluable help in performing the fluid mechanics simulations. Without him, the present study would not have been possible.

I would also like to express my gratitude to Dr. Anargiros Delis and Dr. George Arampatzis, as members of the Thesis Examination Committee.

I also thank my employer, OGT Greentech Ltd. for permission to use the prototype model as study material. Our director, Mr. Seth Larson, and all colleagues. Especially I would like to thank Dr. Mark Venton for his technical and moral support in this study, as well as in everything we have worked on together.

Last but not least, I would like to thank my wife and life partner for all the sacrifices she made to allow me to complete my studies.

## Table of Contents

Abstract .....	3
Περίληψη.....	5
Acknowledgements .....	7
Chapter 1: Literature review.....	9
Chapter 2: CAD Model.....	18
2.1 Column Design.....	19
Chapter 3: Loading.....	21
Case 1 - Normal External Condition .....	22
Case 2 - Extreme External Condition .....	22
3.1 Computational Fluid Dynamics (CFD) simulations .....	23
3.2 The CFD results for Case 1.....	25
3.3 The CFD results for Case 2.....	25
3.4 Load Distribution.....	28
3.4.1 Force analysis Case - 1 .....	28
3.4.2 Force analysis Case - 2.....	30
Chapter 4: Simulation Setup.....	31
Chapter 5: Meta-analysis .....	39
5.1 Case 1 Results - 18m/s.....	40
5.2 Case 2 Results - 50m/s.....	42
5.3 Modal Analysis.....	45
5.4 Modal Analysis Results .....	46
5.5 Linear Buckling.....	49
5.5.1 Set-up.....	50
5.5.2 Linear Buckling Results.....	50
Chapter 6: Conclusions .....	54
Terminology.....	55
Appendix A - Parts List .....	56
Appendix B - CFD Data.....	59
References.....	61

# Chapter 1: Literature review

In this chapter, we document how other researchers encounter strength analysis and seek to identify best practices and guidelines. The focus of this study is the Diffuser Augment Wind Turbines (DAWTs), but it would be a great mistake to neglect the enormous research effort on the Horizontal Axis Wind Turbines (HAWTs).

In HAWTs the predominant trend is the steel tube superstructure that supports the ever-increasing diameter of the rotor and blades. Many researchers are studying steel tube towers. The possibility of reducing the thickness of the tower by introducing internal stiffening rings was investigated by [Hu, et al., 2014]. Design and analysis of 2 MW and 1.5 MW wind turbines were undertaken by [UMESH, et al., 2016], [Chantharasenawong, et al., 2011], while for a 1 MW turbine by [Huskey and Prascher, 2004] and [Lavassas, et al., 2003].

Dimopoulos and Gantes, presented an experimental study of buckling of cylindrical shells of wind turbine towers with opening and stiffening under bending [Dimopoulos and Gantes, 2012]. Buckling of an opening door with FE was studied by [Tran, et al., 2015].

The combination of FE and a Genetic Algorithm for wind turbine optimization was used by [Wang, et al., 2016]. Nonlinear response history analysis and the collapse study of a wind power tower exposed to tropical cyclones was investigated by [Dai, et al., 2017].

In more detail, the possibility of reducing the thickness of the tower by introducing internal stiffening rings was examined by [Hu, et al., 2014]. They compare a tower without stiffening rings, a tower with stiffening rings, and a third tower with strong rings but with lower wall thickness. This was done for three towers of different heights (50 m, 150 m, and 250 m). The distribution of the fundamental wind pressure over the height of the tower was calculated according to the standard BS EN 1991-1-4. Simplified distribution patterns of wind load are shown in Fig. 1.1.

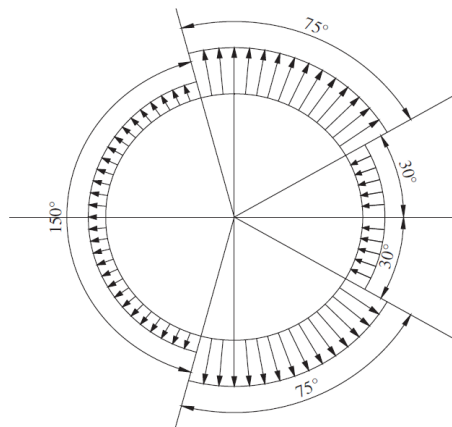


Fig. 1.1 Simplified distribution patterns of the wind loads [BS EN 1991-1-4].

They used the ABAQUS software for the simulations to study horizontal sway and von Mises stress as a function of weight reduction ratios. The shell of a tower is simulated as an S4R shell

element, which is a double-curved thin or thick shell with 4 nodes, and the flange is simulated as a C3D10 continuum element, which is a square tetrahedron with 10 nodes. The constraints are a fixed support on the ground and a connection constraint between the flange and the shell.

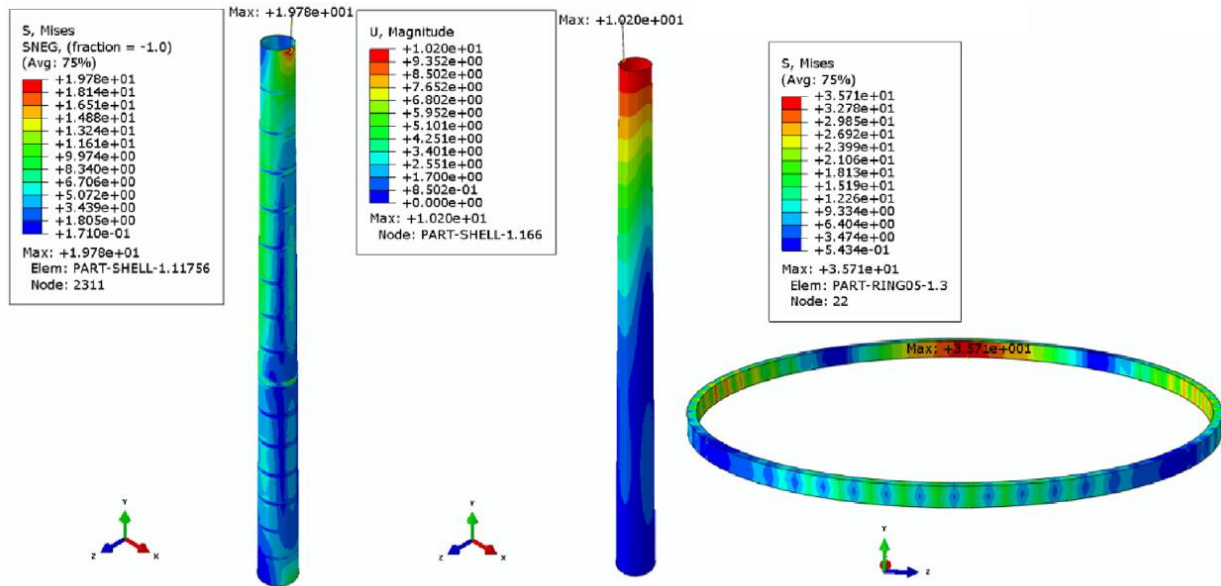


Fig. 1.2 (a) Von Mises stress in the shell (b) Horizontal sway of the shell (c) Von Mises stress in the ring [Hu, et al., 2014].

Their results (Fig. 1.2) show that the stiffening rings contribute to strengthening and specially to reduce buckling, but the material reduction and therefore cost reduction depends on the height of the tower and the density of the rings.

Dimopoulos and Gantes, [Dimopoulos and Gantes, 2012], present an experimental study of buckling of cylindrical shells of wind turbine towers, with opening and stiffening under bending. They investigate the problem of very thin shells buckling under compression more than predicted by analytical calculations. This phenomenon is mainly caused by inelastic effects and geometric imperfections.

They design and conduct their experiments in parallel with finite element numerical analysis. The numerical analysis was performed with ABAQUS, at three different levels of resolution. At the primary level, the presence of bolts was ignored, and the adjacent flanges were "glued" to each other via connection constraints. In the second and third numerical models, the presence of bolts was taken into account, so that the interaction between bolts and flanges and the interaction between flanges were considered. However, in the second model the column was considered as fixed, while in the third model the effects of the non-rigid column were considered by using two springs representing the vertical translational and horizontal rotational stiffness of the column (Fig. 1.3).

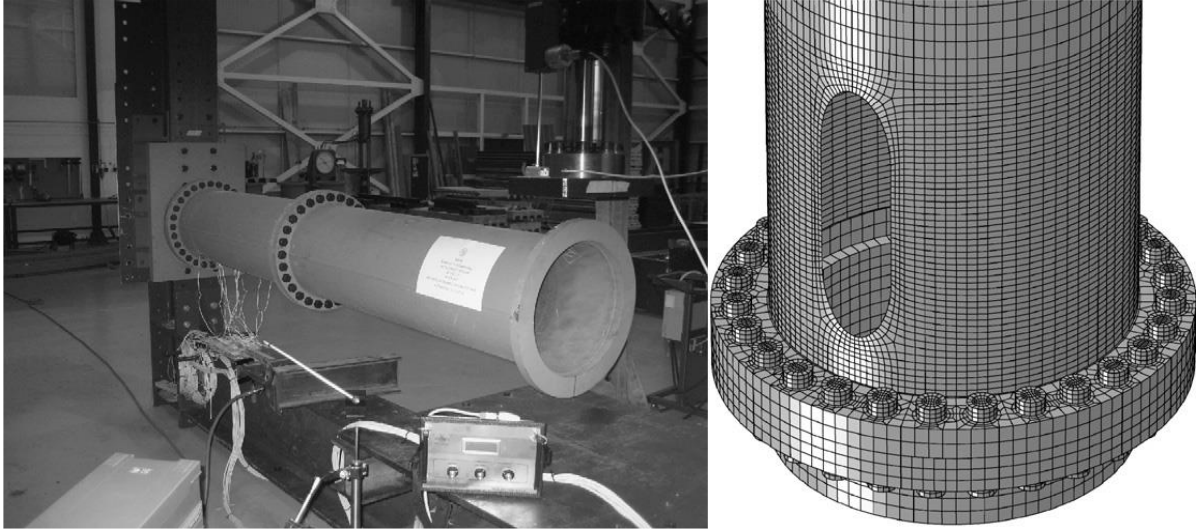


Fig. 1.3 Left: The Experimental configuration; Right: The computer model mesh [Dimopoulos and Gantes, 2012].

The shells were simulated with the shell element S4R, which is a double-curved thin or thick shell with 4 nodes, a finite element with reduced integration and hourglass control capable of calculating finite membrane stresses. The rest of the cantilever model (all flanges and the thick/short cylinder at the support) was simulated with the C3D8R continuum element.

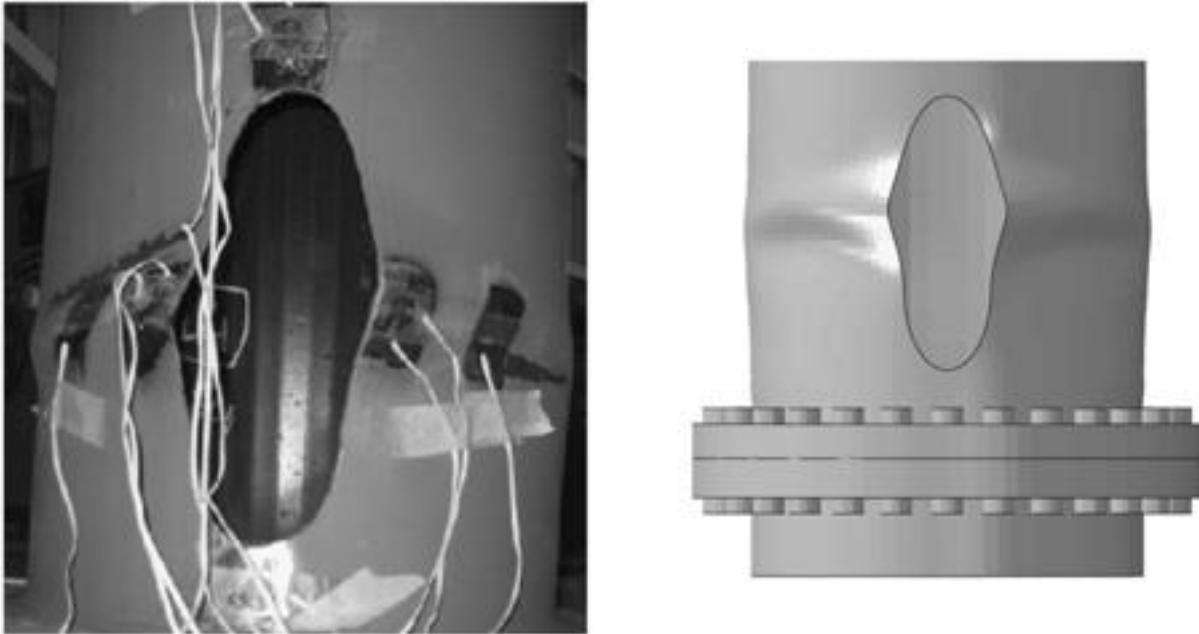


Fig. 1.4 Direct comparison of experimental result and modeling [Dimopoulos and Gantes, 2012].

The experimental results (Fig. 1.4) largely confirm the numerical ones in terms of load-displacement curves and ultimate load. The numerically obtained strains did not correlate well

with the corresponding experimental strains in many cases, mainly due to the presence of initial imperfections that are inevitably present in the specimens [Dimopoulos and Gantes, 2012].

The design of a wind tower for a 2 MW turbine was studied by [Umesh, et al., 2016]. They started with the calculations of the loads, replaced the masses of the nacelle and blades with dead loads, and added the thrust force calculated at maximum wind speed. They defined the loads and moments in each of the three segments of the tower connection flanges. S355 stainless steel, the most commonly used material for wind turbine towers, was chosen as the material of construction. It was modeled in Catia V5 and analyzed with Ansys 14.0, while it was meshed with 418677 tetrahedral elements and 791170 nodes.

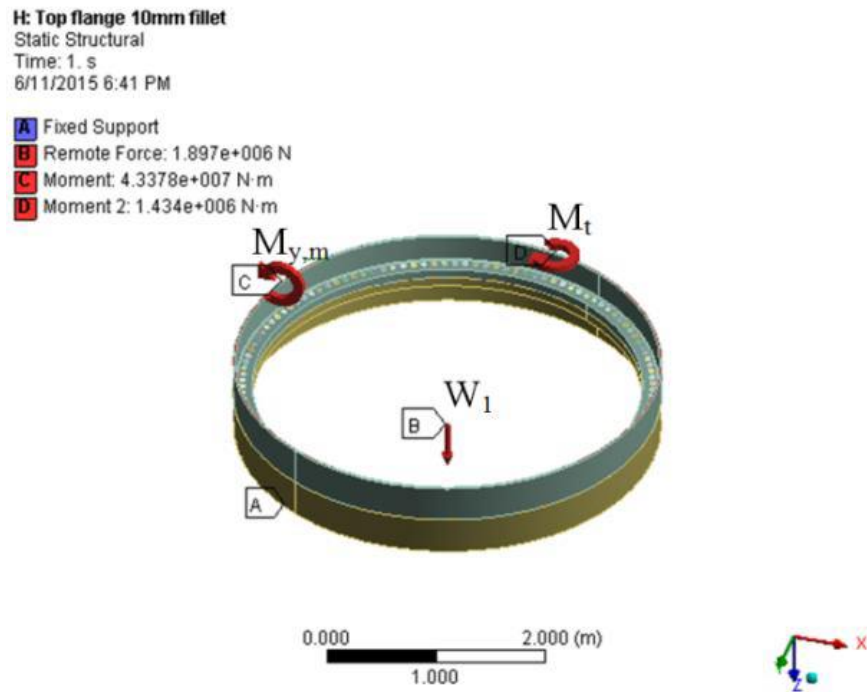


Fig. 1.5 Loads and moments on Middle Flange [Umesh, et al., 2016].

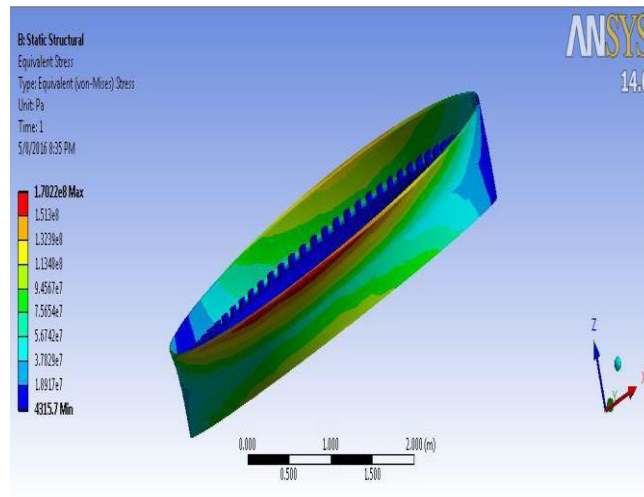


Fig. 1.6 Equivalent Stress in Middle Flange [Umesh, et al., 2016].

They refer to a formula from Lingaiah's book [Lingaiah, 2006] that calculates the number of bolts on a tower when the diameter of the shell is known:

$$\text{Number of bolts} = 0.028 * \text{maximum diameter of shell.}$$

However, they go a step further by using Von Mises failure theory to decide on the stability of the shell thickness and then optimize the number of bolts in each flange connection [Umesh, et al., 2016]. The resulting optimum is 80 bolts, as shown in Fig. 1.7.

Trial No.	Flanges			
	Middle Flange		Top Flange	
	No of bolts	Stress Induced (MPa)	No of bolts	Stress Induced (MPa)
1	120	170	98	174.15
<b>2</b>	<b>100</b>	<b>235.11</b>	<b>80</b>	<b>219.68</b>
3	80	352.32	60	274.77

Fig. 1.7 Optimize the number of bolts [Umesh, et al., 2016].

Fatigue life estimation was performed using the Uniform Material Law (UML) method. UML is a practical and user-friendly method, because only the tensile strength data of the material is required to estimate the strain-life curve (S-N curve) [Umesh, et al., 2016]. The maximum fatigue life is 106 cycles as shown in the Fig. 1.8:

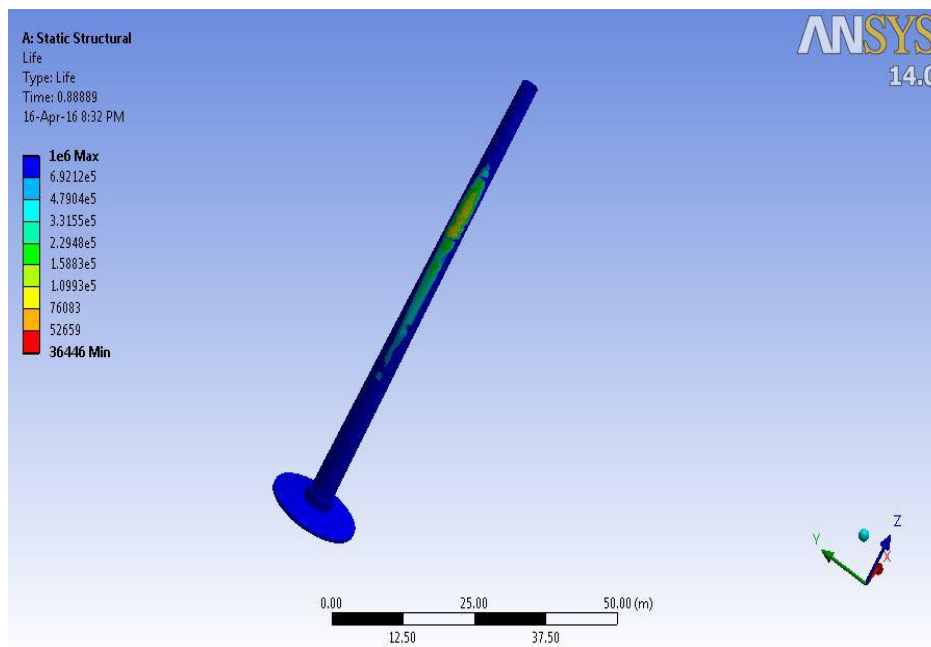


Fig. 1.8 Fatigue Life Analysis [Umesh, et al., 2016].

Finite element analysis was also used by [Chantharasenawong, et al., 2011] to study a modular tapered tubular tower of a 1.5 MW wind turbine in Thailand. From this work, it is worth mentioning that they study the tower as a system and do not study the modular parts individually. The loads were calculated according to IEC 61400-1 and Eurocode 1 for operational and survival conditions.

The analysis was performed with static loads and a linear elastic model. The material used was again S355J2 with a yield strength of 355 MPa. Euler-Bernoulli beam theory was used to predict the deflections and verify the FE models [Chantharasenawong, et al., 2011]. The simulations were performed using ABAQUS commercial software. The mesh consisted of quadrilateral shear deformable shell elements (4-node element), fixed boundary conditions at the base and a rigid plate at the top.

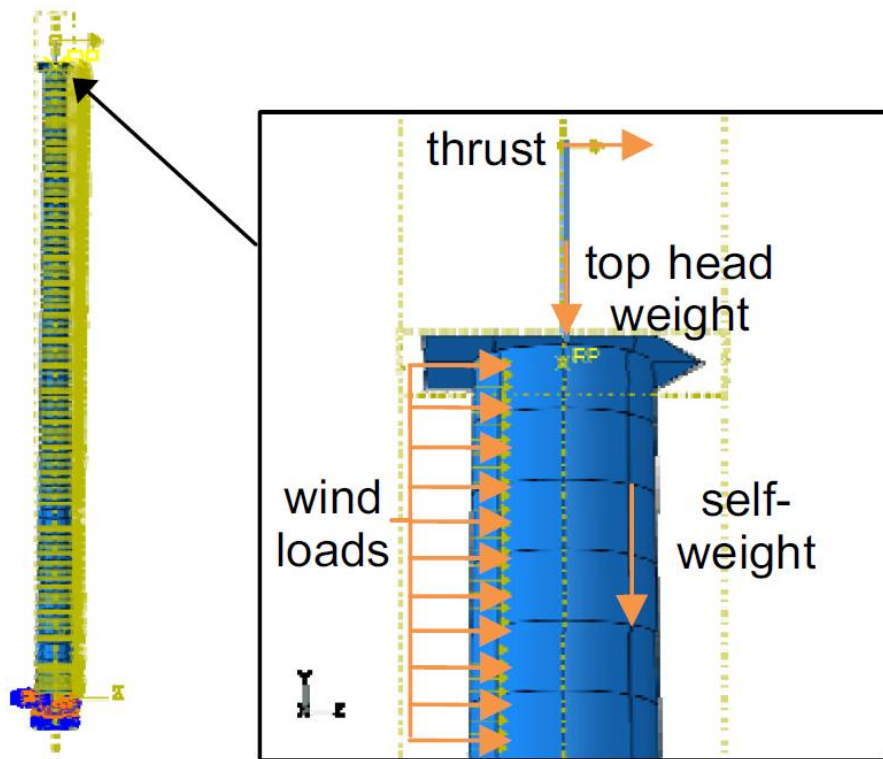


Fig. 1.9 Loads representation [Chantharasenawong, et al., 2011]

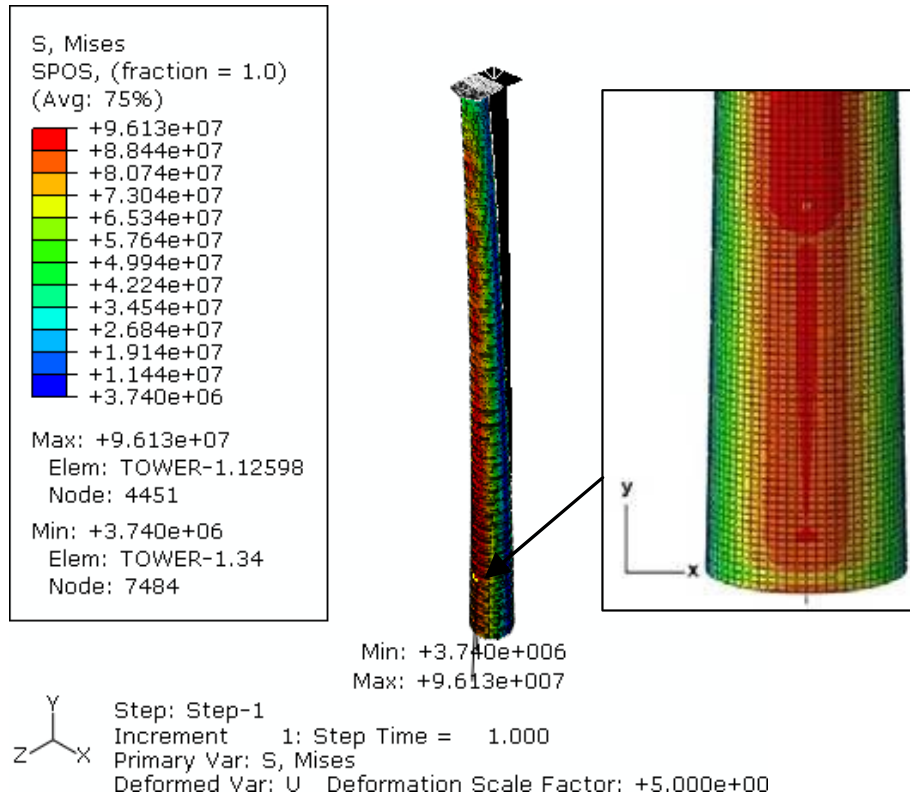


Fig. 2 Von Mises stress distribution [Chantharasenawong, et al., 2011].

Gravity loads come from the tower's own weight and from the rotor, nacelle, and blades on the top flange. Aerodynamic loads come from rotor torque at higher power on cutout speed and from direct aerodynamic pressure on the tower surface.

Buckling analysis was critical due to the modular tower design, larger diameter, and thinner walls. According to the authors [Chantharasenawong, et al., 2011], when the shell thickness is reduced and the diameter is increased, the local buckling becomes the dominant criterion instead of the maximum stress. The finite element buckling analysis was verified using Euler's buckling formula for a cylindrical model:

$$P_{cr} = \frac{\pi^2 EI}{L_e^2}$$

where  $P_{cr}$  is the critical buckling load, while  $L_e$  is the effective length.

A comparative study of singular straight and a tapered monopole tower for a domestic wind turbine was carried out by [Patel and Ramani, 2017]. Using the same tower height of 12.5 m, thickness of 5 mm, and weight of 1842 kg, they compare a straight cylindrical tower with an outer diameter of 1.2 m to a tapered tower with 1.4 m at the bottom and 1 m at the top. For the load calculations, the authors recommend using simplified methods from several available methods described in the RISØ guidelines [Riso, 2002].

For their study, they use ANSYS Workbench for static structural analysis, modal analysis, and linear buckling analysis. Both modeling methods, shell element and solid element, are used for comparison. They show that the shell element method gives identical results to the solid element method, but with significantly less computational effort and time [Patel and Ramani, 2017].

The following results are clearly in favor of the tapered tower with lower total deformation and lower Normal and von Mises stress. The tapered tower has a higher Natural frequency value with lower probability of resonance in the structure.

	<b>Tapered hollow monopole</b>	<b>Straight hollow monopole</b>
<b>Total Deformation max (mm)</b>	7.709	9.895
<b>Normal Stress max (MPa)</b>	22.111	31.858
<b>Normal Stress min (MPa)</b>	-25.226	-34.596
<b>von-Mises Stress max (MPa)</b>	19.486	26.898
<b>von-Mises Stress min (MPa)</b>	0.105	0.177
<b>Linear Buckling Load Multiplier</b>	47.148	44.515
<b>Natural Frequency (Hz)</b>	9.127	7.514
<b>Weight (Kg)</b>	1842	1842

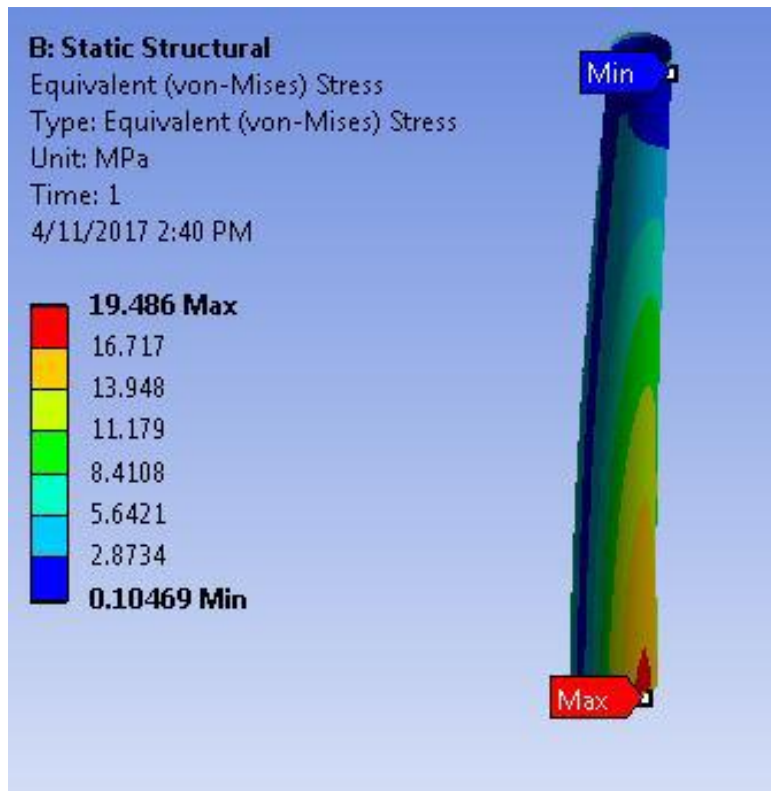


Fig. 1.11 Von-Misses Stress of Tapered monopole [Patel and Ramani, 2017].

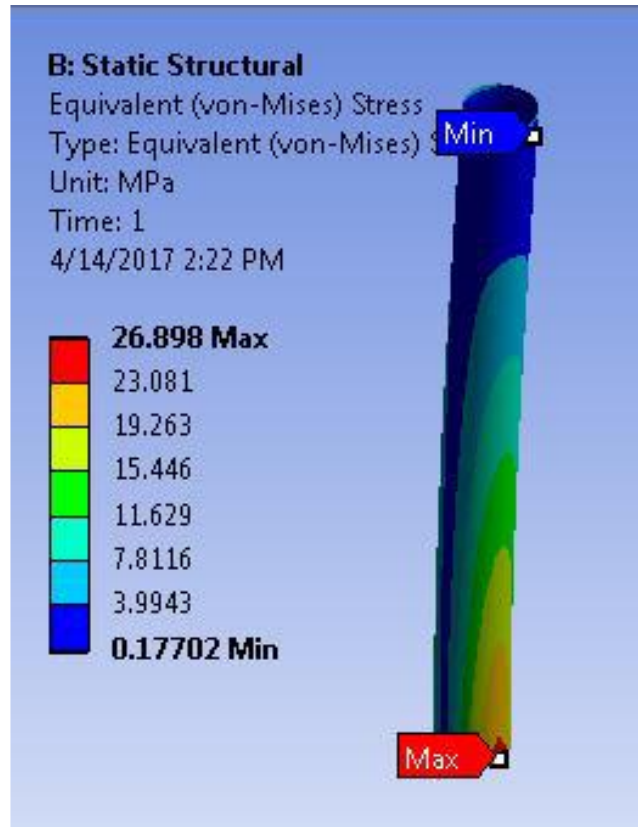


Fig. 1.12 Von-Misses Stress of Straight monopole [Patel and Ramani, 2017].

# Chapter 2: CAD Model

The design was created with the aim of constructing a metal frame strong enough to hold the diffuser under the following constrains.

- To be able to be manufactured from materials readily available on the market, such as metal profiles, metal sheet, etc.
- To be technically feasible for construction.
- To have the least possible resistance on direct airflow.
- To have the minimum weight.

The design software used was the Autodesk's Inventor 2021. The 3D model represents the structure in 1:1 ratio. It contains the frame parts, the stiffener flanges, and the welds in detail. The *Frame Generator* tools were used to import the main column, while the rest of the flanges were made in separate pieces, as Sheet metal parts. The welds were made with the "Welding" tool, where it recognizes the contact surfaces, treat the edges, and can add welds with specific characteristics.

The target of the study was only to exam the main metallic column, located in the center of the diffuser, as shown in Fig. 2.1. The rest of the parts were removed and replaced with the corresponding forces.

In the model extracted for the simulation, some elements, which are not structurally involved in the structure, were removed to simplify the simulation. The exact geometries of the structural elements and welds were kept. The model to be simulated is exported in neutral CAD format, Parasolid Model File (x\_b).

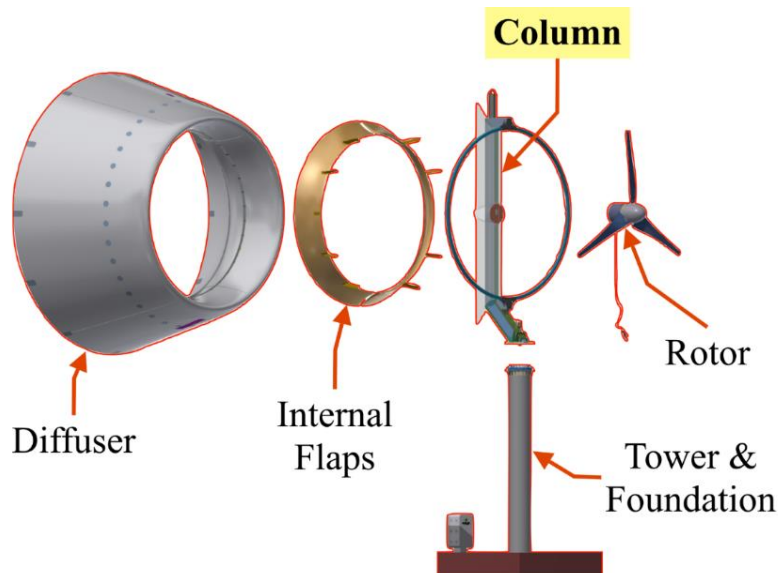
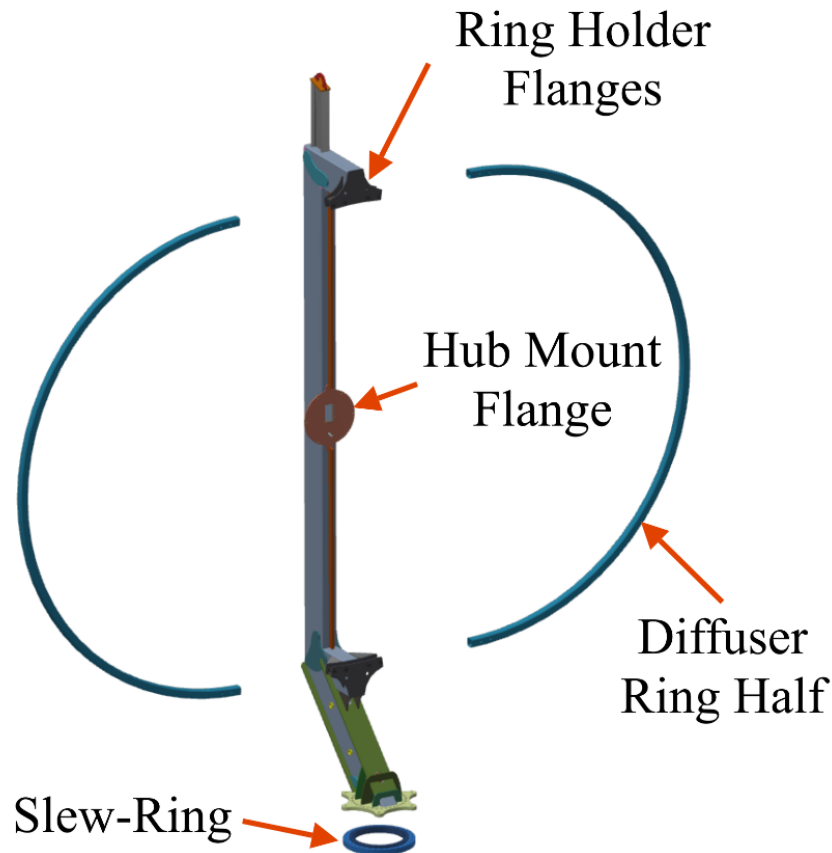


Fig. 2.1 The column being the subject of this study.

## 2.1 Column Design

The design of the central column is such that it supports the upper structure while rotating 360° in the wind direction. The first section of the column is inclined at 45° to move the center of pressure of the diffuser to the rear. In this way, the diffuser acts as a rudder, passively steering the turbine in the wind direction, without the need for a yaw mechanism.



*Fig. 2.2 Mounting Flanges for connections.*

There are three points of contact between the column and the rest of the structure.

- The slew-ring is mounted to the underside.
- The hub, consisting of the motor and the blades, is attached to the flange in the center of the column.
- The diffuser, which is mounted around a hollow 100x100x10 metal tube formed into 2 semicircles. The 2 semicircles are held together with bolts between 2 flanges above and below the center of the diffuser (Fig. 2.2).

All three contact points in the simulation are replaced by the corresponding forces. The bearing flange is pressed in as a fixed element. The rotor transmits force and torque to the bearing flange.

And the diffuser transfers all forces to the holding flanges. The diffuser ring itself is not involved in the analysis.

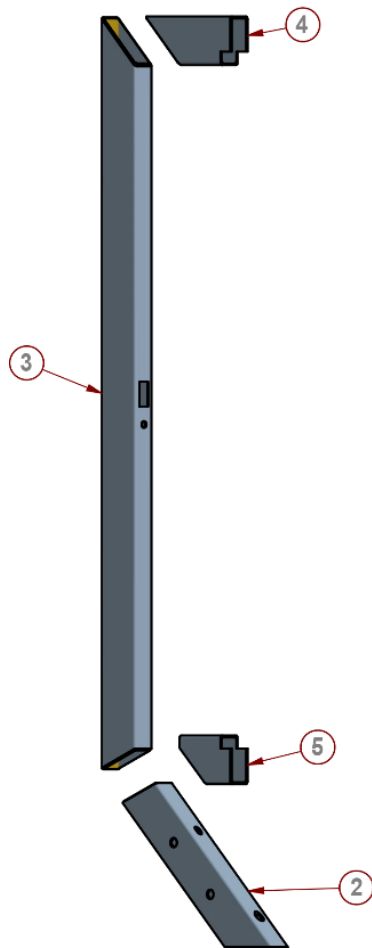


Fig. 2.3 Column Main parts.

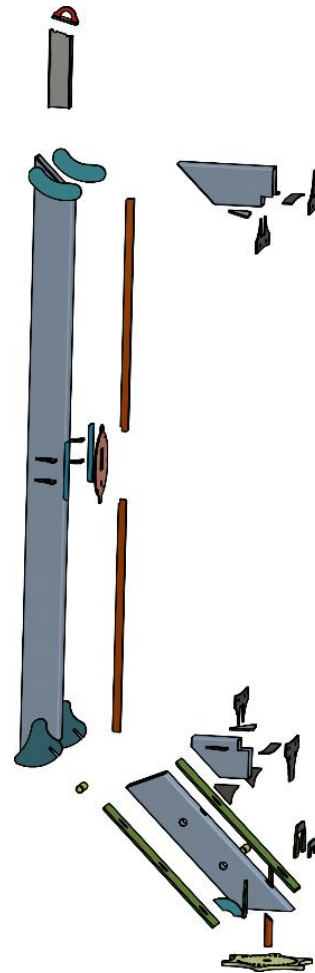


Fig. 2.4 Column Exploded view

In detail, the core of the column consists of 400x200x16 tubular beams. The hollow beam was chosen for its ability to carry both bending and torsional loads. Since it distributes the material away from the symmetry axes  $XX'$   $YY'$ , it has higher Elastic Section Modulus values. The greater the section modulus, the greater the forces required to bend the beam.

The remaining flanges and stiffeners are made of plates of various thicknesses. All elements are joined by welding, according to the ISO/TS 20273:2017 standard.

The final column is a single piece painted or galvanized to prevent rust. The total weight of the column including welds is 1984,25 kg.

The Bill of Materials (BOM) of all parts that participate in analysis can be found in *Appendix A – Parts List*.

# Chapter 3: Loading

To calculate the loads, we must first determine the operating conditions. Weather conditions vary mainly depending on the geographic location of the turbine. For our theoretical study, we will be guided by the IEC 61400-2:2013 Standard. The Standard defines the extreme weather conditions that a wind turbine should withstand. In addition, we will also study the case where the wind turbine has reached its maximum operating potential.

The main forces to which the wind turbine is subjected are:

- The weight of the structure
- The wind pressure on the front surface, which is determined by the wind direction. This includes all surfaces of the diffuser, the column and actuator disc.
- The torque generated by the blades when they meet the resistance of the motor, resistance opposing their direction of rotation.

The weight can be calculated from CAD drawings, since we know the materials and the densities, we know the weights of each part. The CAD software can also give us the point where the center of gravity is located. As we will see later, the center of gravity is outside the column, but this is not a problem. In the structural simulation there is a way to connect it to the structure.

Wind pressure creates a force known as drag. The drag force has no straightforward analytical method for estimation. The only accepted method that has gained industry acceptance is CFD (Computational Fluid Dynamics). These simulations were performed in the Turbomachines & Fluid Dynamics Laboratory (TurboLab-TUC), School of Production Engineering & Management, Technical University of Crete, by Stavros Leloudas. The CFD numerical results can be found in Appendix B – CFD Data.

The torque can be calculated if the maximum theoretical power of the motor is known. Therefore, as we mentioned earlier, we consider two cases for determining the load. The first case is the maximum operating speed of the wind turbine, at which the rotor rotates at the maximum permissible speed. The second case refers to the extreme external conditions.

	<b>Case 1 - NEC (Normal External Condition)</b>	<b>Case 2 - EEC (Extreme Condition)</b>	<b>External</b>
<i>Free Stream Velocity</i>	18 m/s	50 m/s	
<i>Rotor angular speed</i>	300 rpm	0 rpm	
<i>Pitch Angle</i>	0°	80°	

## Case 1 - Normal External Condition

In this case, the turbine operates at maximum load (cutoff speed), which is 18m/s. The generator runs at a maximum rotation of 300 rpm and generates 15 KW of energy. This results in a corresponding torque on the motor's bearing flange of the tower. The torque is calculated as follows:

$$\text{The angular speed is: } \omega = \frac{2\pi \cdot 300 \text{rpm}}{60\text{s}} = 31.4 \text{ rad/s}$$

$$\text{The Torque is: } N = \frac{P}{\omega} = \frac{15 \text{ kW}}{31.4 \text{ rad/s}} = 477.7 \text{ Nm}$$

Other parameters that are need for CFD analysis are:

Turbulence intensity was set to 10%.

Tip Speed Ratio (TSR) is calculated using the following formula:

$$TSR = \frac{R \cdot \omega}{v} = \frac{2.7\text{m} \cdot 31.4\text{rad/s}}{18\text{m/s}} = 4.71$$

## Case 2 - Extreme External Condition

In this case, we are first asked to determine the wind speed. We will be guided by the IEC 61400-2:2013 Standard. According to this standard, wind turbines are classified into 5 categories depending on the wind potential of the site, Fig. 3.1. We aim for Category I, for a maximum speed of 50 m/s. The rotor blades are in the feathering position and theoretically have no rotational speed, and therefore no torque on the flange.

**Table 1 – Basic parameters for SWT classes**

SWT class	I	II	III	IV	S
$V_{ref}$ (m/s)	50	42,5	37,5	30	Values to be specified by the designer
$V_{ave}$ (m/s)	10	8,5	7,5	6	
$I_{15}$ (Note 2) (-)	0,18	0,18	0,18	0,18	
$a$ (-)	2	2	2	2	
NOTE					
1) the values apply at hub height, and;					
2) $I_{15}$ is the dimensionless characteristic value of the turbulence intensity at 15 m/s, where 0,18 is the minimum value that shall be used, and noting that Annex M discusses observations regarding turbulence intensity;					
3) $a$ is the dimensionless slope parameter to be used in Equation (7).					

Fig. 3.1 Table 1 from chapter 6.2 of standard IEC 61400-2:2013.

Therefore, it is now the time to perform CFD to calculate the drag forces for both cases.

### 3.1 Computational Fluid Dynamics (CFD) simulations

Computational Fluid Dynamics (CFD) is the most reliable and widespread method for calculating flow phenomena. However, its implementation requires experience and deep knowledge of the subject matter. The analysis for our study was performed by Stavros Leloudas under the supervision of Prof. Ioannis Nikolos, at Turbomachines & Fluid Dynamics Laboratory - TUC. The detailed results are given in Appendix B - CFD Data.

The simulation method was performed by solving the incompressible 3D Reynolds-Averaged Navier-Stokes (RANS) equations. The turbulence simulation was performed using the Shear Stress Transport (SST) two-equation turbulence model.

The mesh is a hybrid-unstructured one, consisted of:

- Triangles      150 102
- Prisms         36 052
- Total cells     186 154
- Total Points   112 274

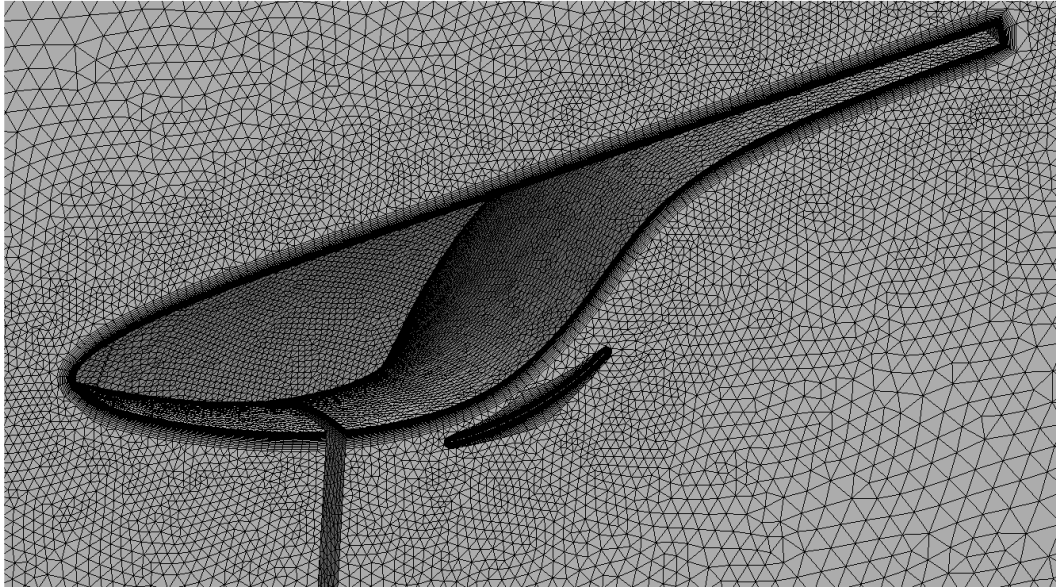


Fig. 3.2 A close-up of the utilized hybrid mesh of the flow domain around the diffuser (indicative picture).

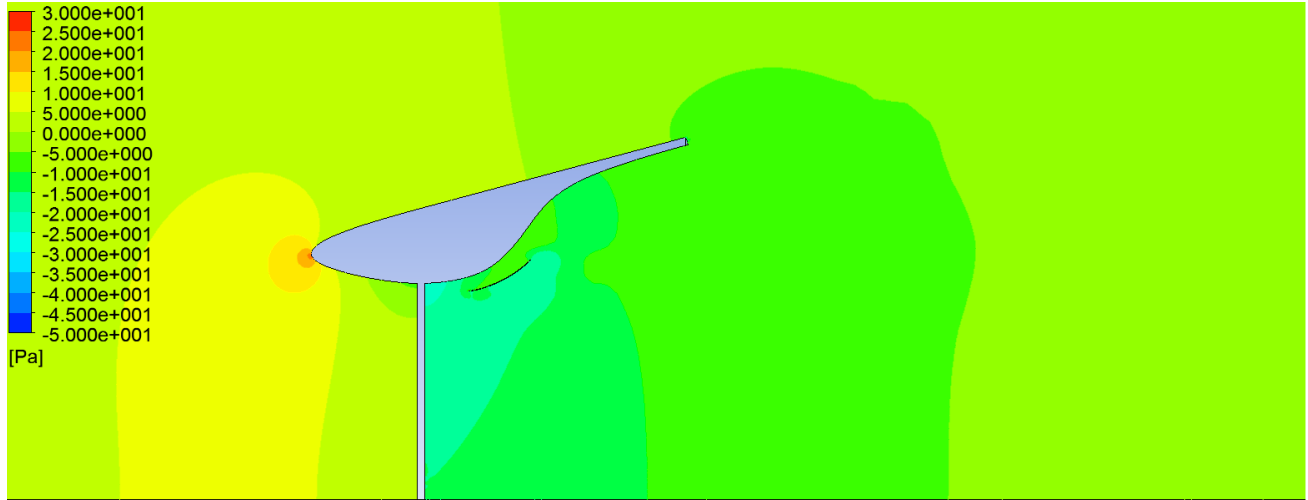


Fig. 3.3 Velocity contours at the symmetry plane (Indicative picture).

### 3.2 The CFD results for Case 1

Case 1 - Normal External Conditions						
Ambient Velocity - $V_o$ [m/s]	Density - $\rho$ [kg/m <sup>3</sup> ]	-	Dynamic Viscosity - $\mu$ [Ns/m <sup>2</sup> ]	RPM	TSR	
18.0	1.200		0.000018	300	4.7141	

Diffuser - Drag [N]	Internal Flap - Drag [N]	-	Rotor Thrust [N]	Total Force [N]	Axial
4582.47	1558.69		2679.35	8820.52	

The table above shows in detail the frontal forces in the 3 sections of the wind turbine, the diffuser, the internal flaps, and the rotor. The total sum force is 8820N, which is approximately equal to 0.9 Ton force.

### 3.3 The CFD results for Case 2

Case 2 - Extreme External Conditions						
Ambient Velocity - $V_o$ [m/s]	Density - $\rho$ [kg/m <sup>3</sup> ]	-	Dynamic Viscosity - $\mu$ [Ns/m <sup>2</sup> ]	RPM	TSR	
50.0	1.2		0.000018	No rotor	-	

	Diffuser - Drag [N]	-	Internal Flap - Drag [N]	Rotor Thrust [N]	Total Force [N]	Axial
No conversion	-		-	0.00	0.00	

In this case, the algorithm has not converged to one value, but as can be seen in the following graph (Fig. 3.4), there is "oscillatory convergence" (unsteady flow, almost periodic).

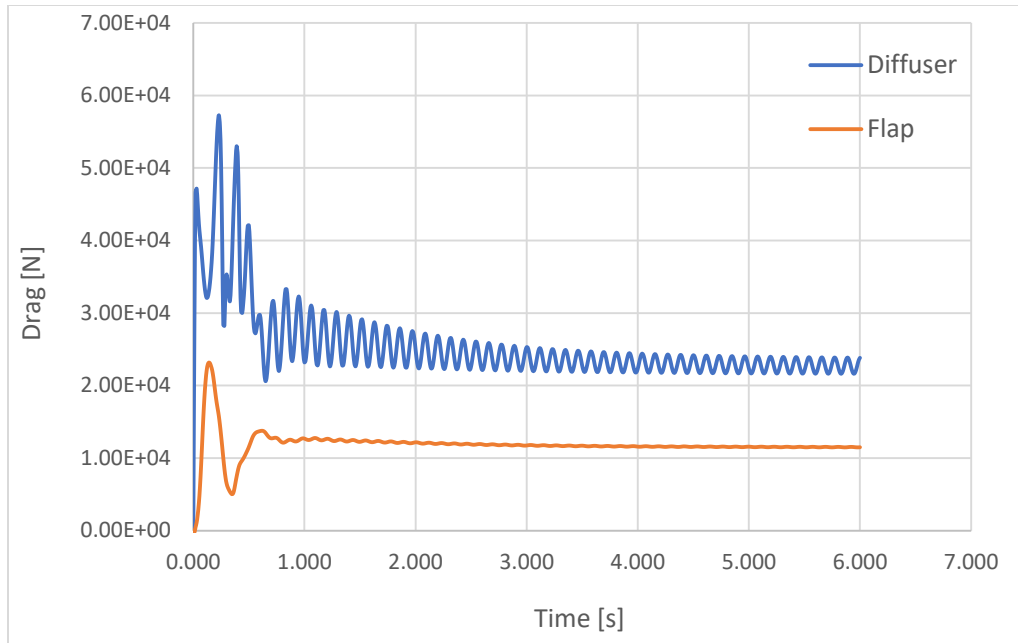


Fig. 3.4 Conversion graph for Case 2 CFD.

Therefore, we break-down the results. We isolated the last second (5s to 6s), where the oscillation seems to stabilize.

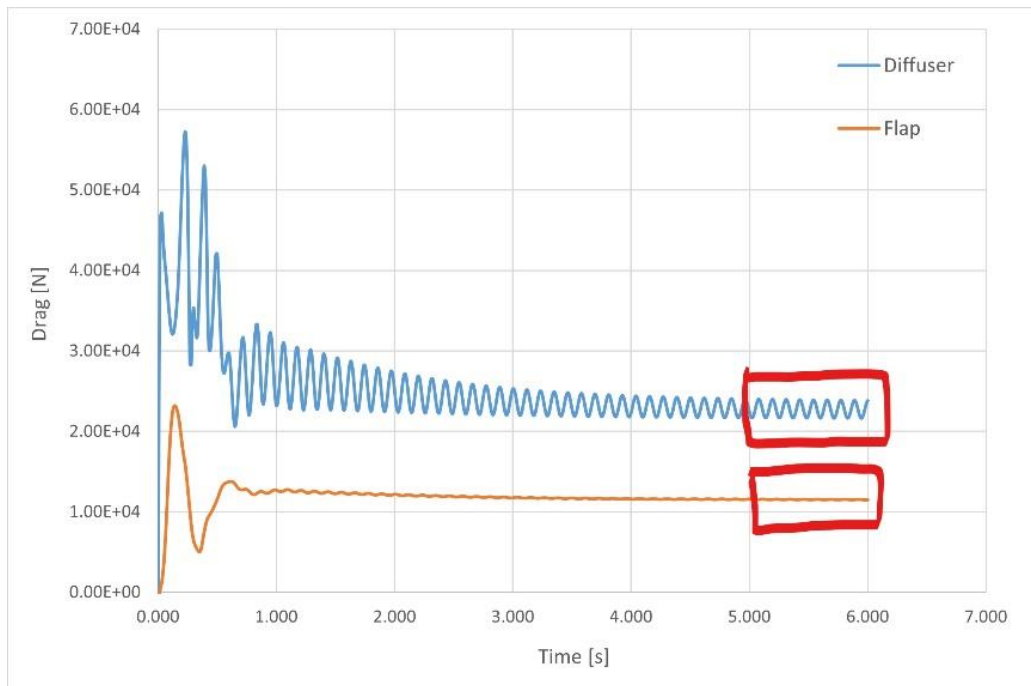


Fig. 3.5 Highlighting the values that seem to be stabilized.

We then connected the peaks and valleys to see the trend of that last second. The trend shows convergence, but at a very slow rate. We also observe a phase delay in the pick time between the diffuser and the flaps, but at the same frequency. The frequency is 8.6 Hz.

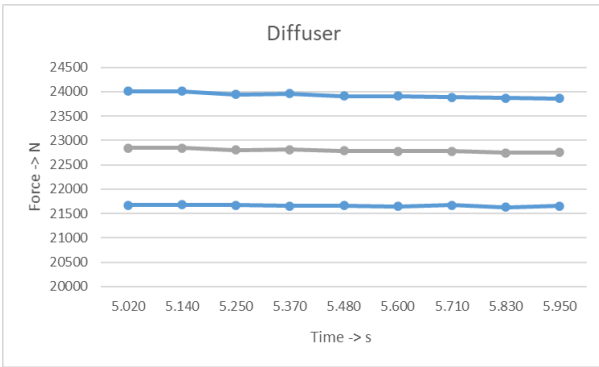


Fig. 3.6 Force convergence trend for Diffuser.

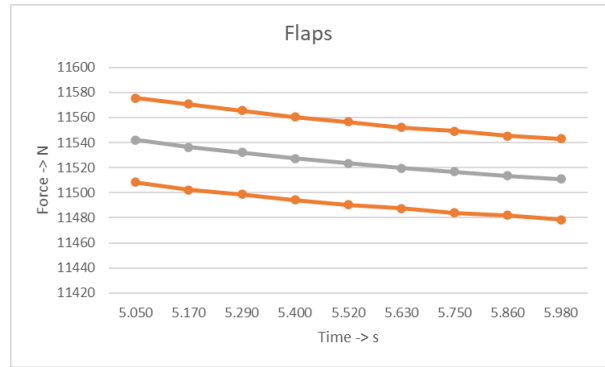


Fig. 3.7 Force convergence trend for internal Flaps.

As the finite Force, we chose the average of the peaks rather than averaging the whole spectrum, just to be on the safe side.

### 3.4 Load Distribution

According to IEC 61400-2:2013, a safety factor of 1.35 is also added to the calculated forces if this applies to a simulation model.

**Table 7 – Partial safety factors for loads**

Load determination method (see 5.2)	Fatigue loads, $\gamma_f$	Ultimate loads, $\gamma_f$
1. Simplified equations	1.0	3.0
2. Simulation model	1.0	1.35
3. Full scale load measurement	1.0	3.0

Tab. 3.1 Table 6 from chapter 7.8.1 in standard IEC 61400-2:2013.

#### 3.4.1 Force analysis Case - 1

The forces as they are formed after the addition of the safety factor:

	Diffuser - Drag [N]	Internal Flap - Drag [N]	Rotor Thrust [N]	Total Axial Force [N]	Rotor Torque [Nm]
	4582.47	1558.69	2679.35	8820.52	477.7
+ Safety factor 1.35	6186.34	2104.24	3617.12	11907.70	643.95

The following Fig. 3.8 shows the forces at the points where they are exerted.

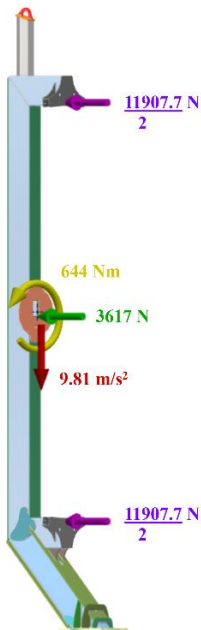


Fig. 3.8 Load distribution for Case 1.

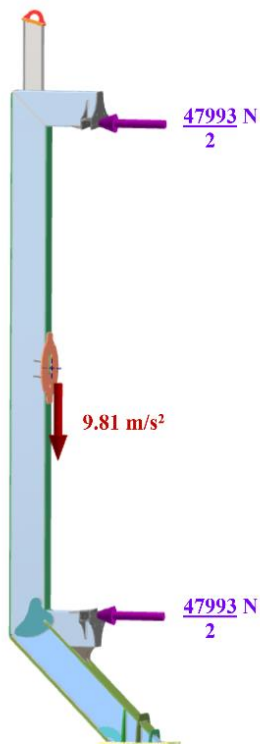
At the bearing joints of the diffuser ring, the drag force of the diffuser and internal flaps is  $(6186.34 + 2104.24 = 8290\text{N})$ .

On the bearing flange of the motor, the rotor thrust is  $3617\text{N}$ . Moreover, in the same flange we have the torque of the motor equal to  $644\text{Nm}$ .

The diffuser and the rotor are replaced by the equivalent forces on their corresponding mounting surfaces. The mass of the diffuser and rotor is replaced by a concentrated mass at their centers of gravity. Gravity acts vertically downward on both the mass of the column and the mass of the diffuser.

### 3.4.2 Force analysis Case - 2

	Diffuser - Drag [N]	Internal Flap - Drag [N]	Rotor Thrust [N]	Total Axial Force [N]
No conversion	-	-	0.00	0.00
Pick values	24000	11550	0.00	35550
+ Safety factor 1.35	32400	15593	0.00	<b>47993</b>



At the mounting surfaces of the diffuser ring, the drag force of the diffuser and internal flaps is 47993N. We assume that in this case with the blades feathered - we have no forces or moments on the rotor flange.

For gravity, the same applies as in Case 1.

Fig. 3.9 Load distribution for Case 2.

# Chapter 4: Simulation Setup

After we have gathered all the necessary information and calculated all the forces, we can start preparing the simulation.



Fig. 4.1 Splitting model in half for X-Plane Symmetry.

First, the design is imported into the software NASTRAN, and we divide the model in half. In this way we get advance of the X-Plane symmetry. This means half mesh, half nodes and half calculations and time.

We set the type of analysis as "Linear Static ". Checking the SPC (Single Point Constraint) option which constrains one or more DOFs from certain movements at a node.

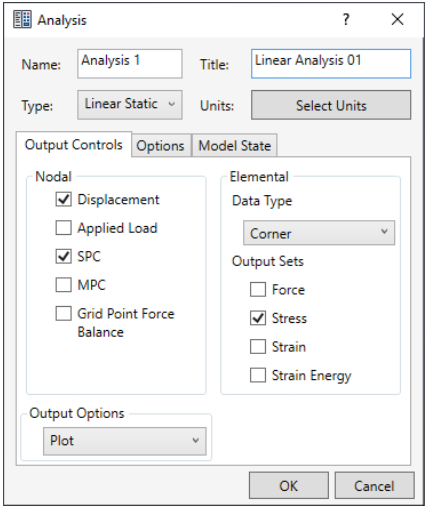


Fig. 4.2 Type of Analysis Linear Static.

The Contact Type option specifies how the touching surfaces of two objects should be connected. We choose 'Bonded' as the global option and then change the type to surfaces that are touching but not connected.

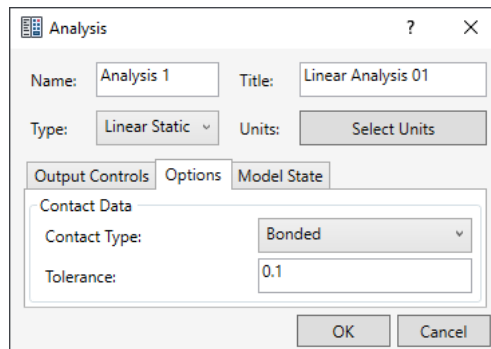


Fig. 4.3 Analysis Options.

The software automatically detects 324 surface contacts and sets the type 'Bonded'. Surfaces that are not bonded and only touch each other should be changed to 'Separate'. In this way, one object cannot penetrate another, but if there are repulsive forces, the 2 objects will be separated and pulled apart.

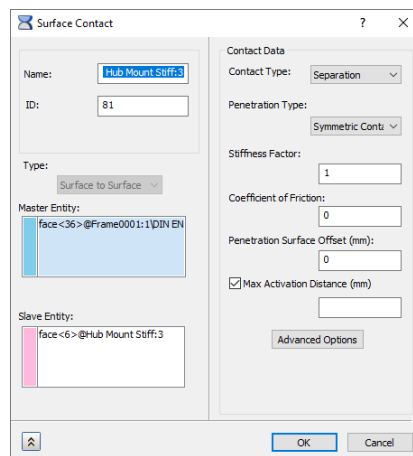


Fig. 4.4 Surface contact.

Moving on to the configuration of the analysis, we begin with the choice of materials. The main structure (frame and flanges) will be made of mild steel ST37 (Fig. 4.5). The welds will be made of another material with higher strength. The choice is MC-50T (Appendix C) from the welding material manufacturer CS HOLDINGS CO. The MC -50T is a mild steel welding wire welded with MAG (Metal Active Gas) with 100% CO2 shielding gas (Fig. 4.6).

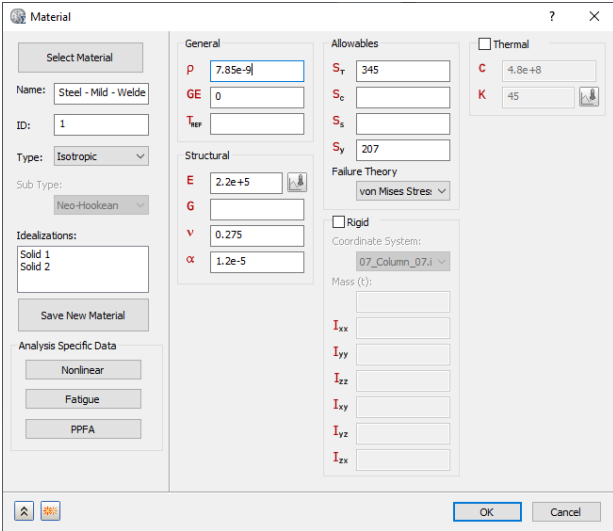


Fig. 4.5 Material properties for main structure.

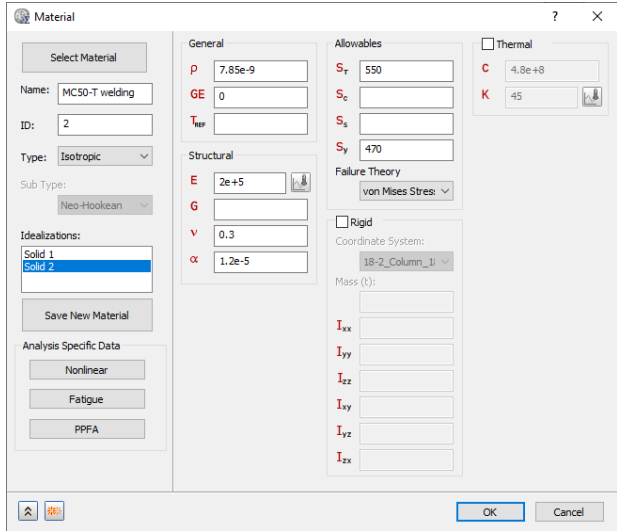


Fig. 4.6 Material properties for the welding.

**Constraints:** We mount the bearing flange to the Slew-Ring with bolts. We allow only one degree of freedom. The rotation is defined only around  $R_y$ , because the bearing can rotate in this direction. The contact points are the Slew Ring on the bottom of the flange (only the contact ring) and the washers of the bolts on the top.

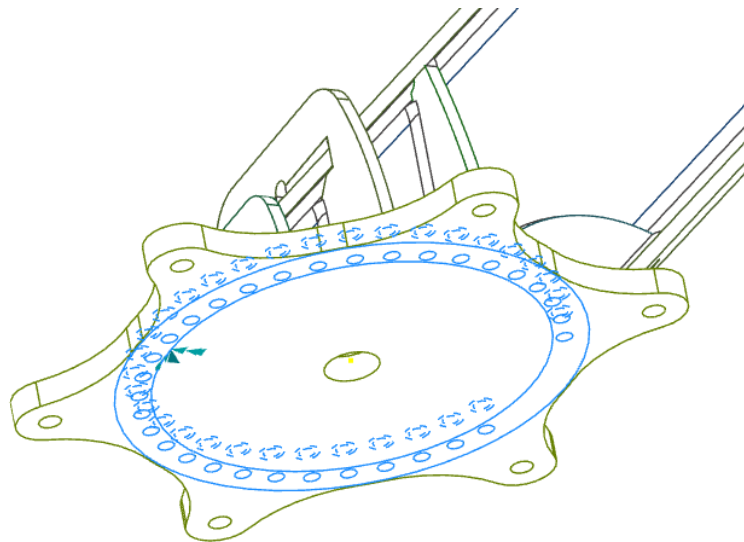
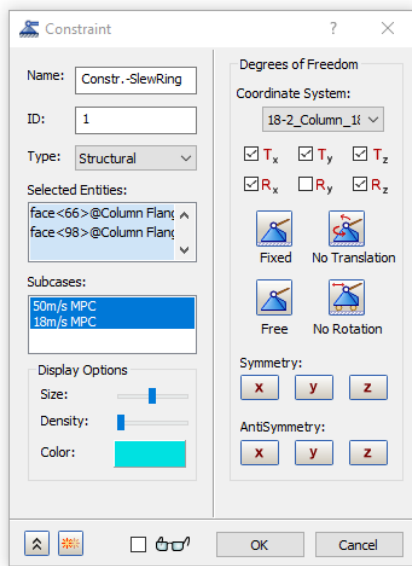


Fig. 4.7 Constraints the mount flange.

**Concentrated Masses:** The masses of the diffuser and rotor are replaced by a concentrated mass at the center of gravity. The mass of the diffuser is 2168.69 kg and for the rotor is 715.45 kg. Combined are equal to 2884.15 kg (2.8 tones).

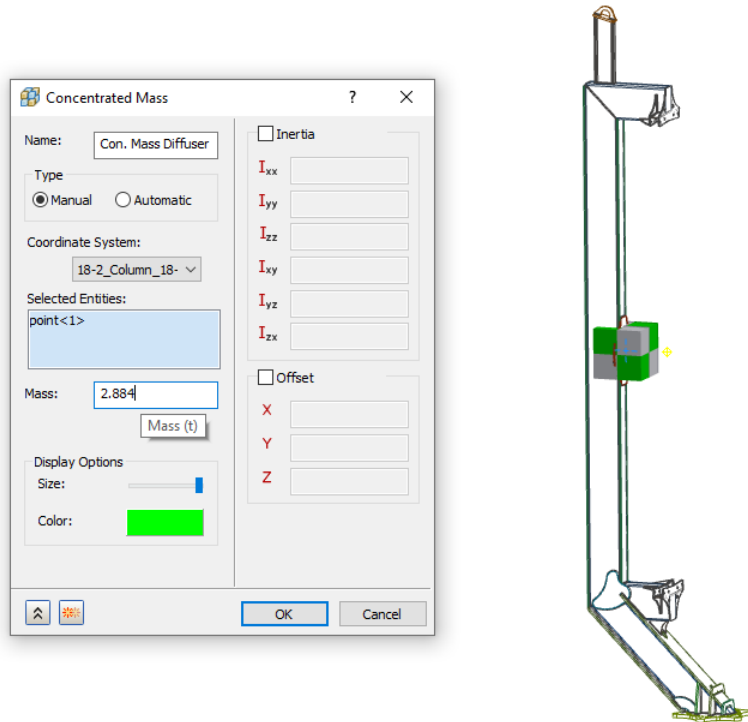


Fig. 4.8 Replace external masses with an equally concentrated mass.

**Connector:** The concentrated mass of the diffuser and rotor are connected by a rigid joint to the bearing flanges of the diffuser retaining ring. This serves 2 purposes. The first is to transfer the gravity of the diffuser, which is considerable and should not be neglected. The second purpose is to transfer the rigidity of the diffuser to the column. This is achieved by the "Rigid Body" option, which does not allow the links to buckle. In fact, the movement and rotation are not limited to one axis, since the diffuser can (and does) move along with the column in any oscillation.

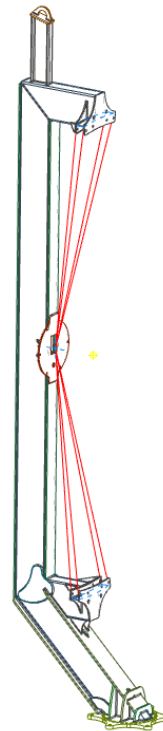
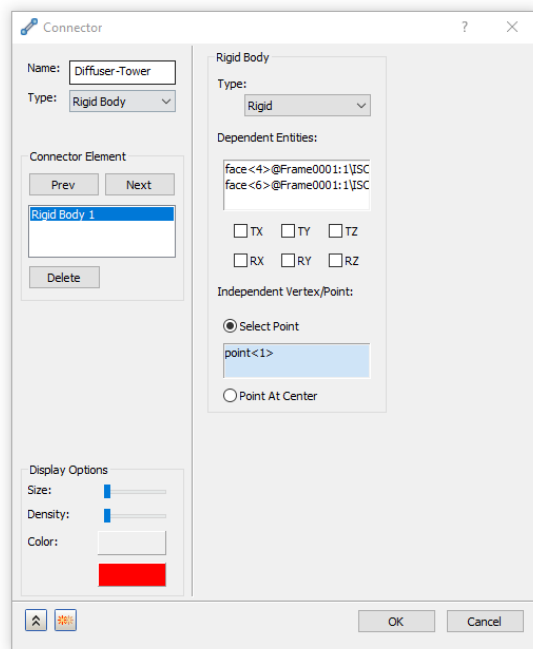
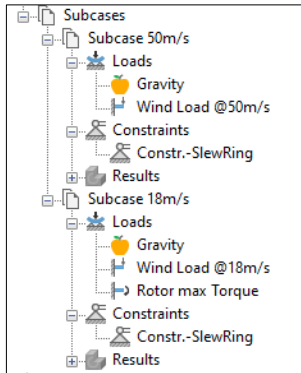


Fig. 4.9 Rigid Connector [External mass – Main structure].

**Loads:** We create two 'Subcases' for the two load cases, as explained above. For each case, we apply the loads as shown in Fig. 4.10.



The constraint conditions and gravity are the same in both cases. The wind load acts on the mounting flanges of the ring in both cases, but with different magnitudes. The torque for case 2 acts on the mounting flange of the rotor.

Fig. 4.10 Subcases.

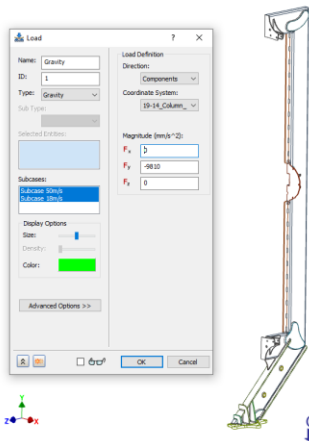


Fig. 4.11 Gravity apply for both cases 1 & 2.

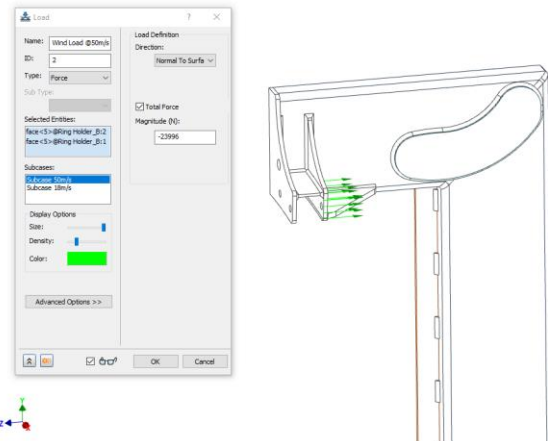


Fig. 4.12 Axial Force for case 2 (4.7 kN total).

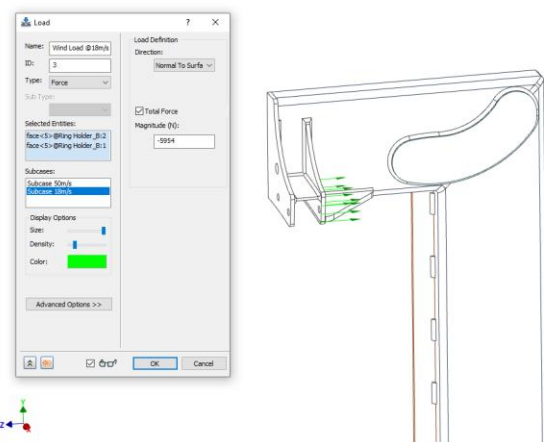


Fig. 4.13 Axial Force for case 1 (1.1 kN total).

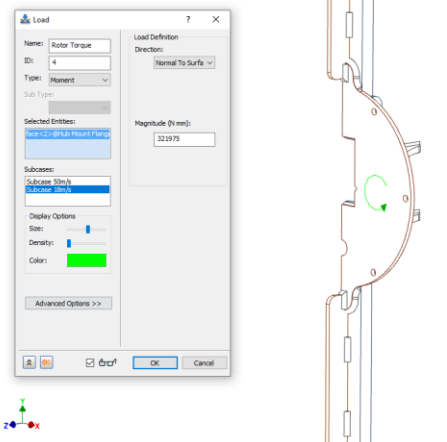


Fig. 4.14 Torque for case 2 (0.6 kNm total).

## Mesh

To create the mesh, we use parabolic elements with an average diameter of 25 mm. Through trials and constant tweaking of the mesh, we have found the parameters that produce the mesh with the best properties, as shown in Fig. 4.15 and Fig. 4.16.

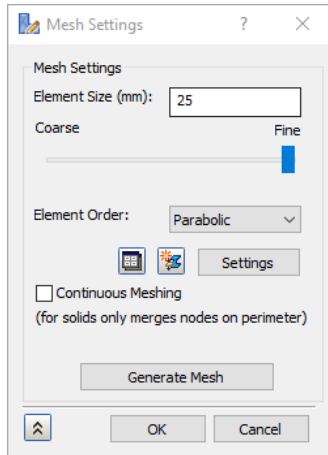


Fig. 4.15 Mesh Settings.

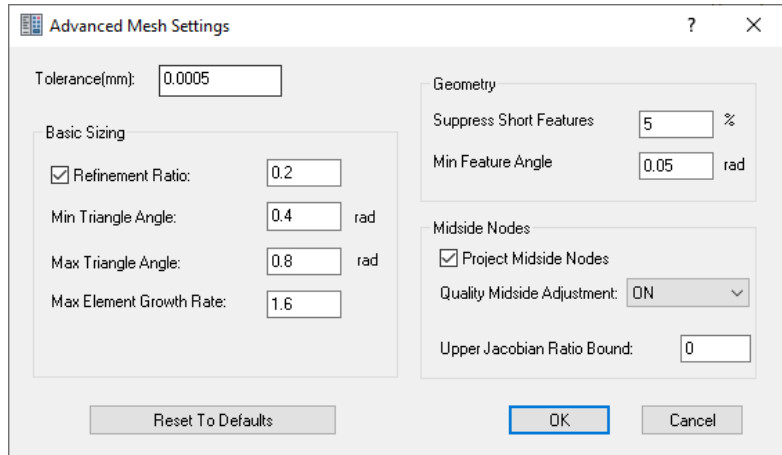


Fig. 4.16 Advance Mesh Settings.

The final mesh consisted of 262794 nodes and 124170 elements. A mesh check revealed zero defects (Fig. 4.17).

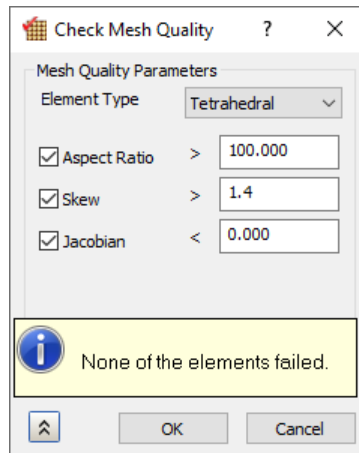
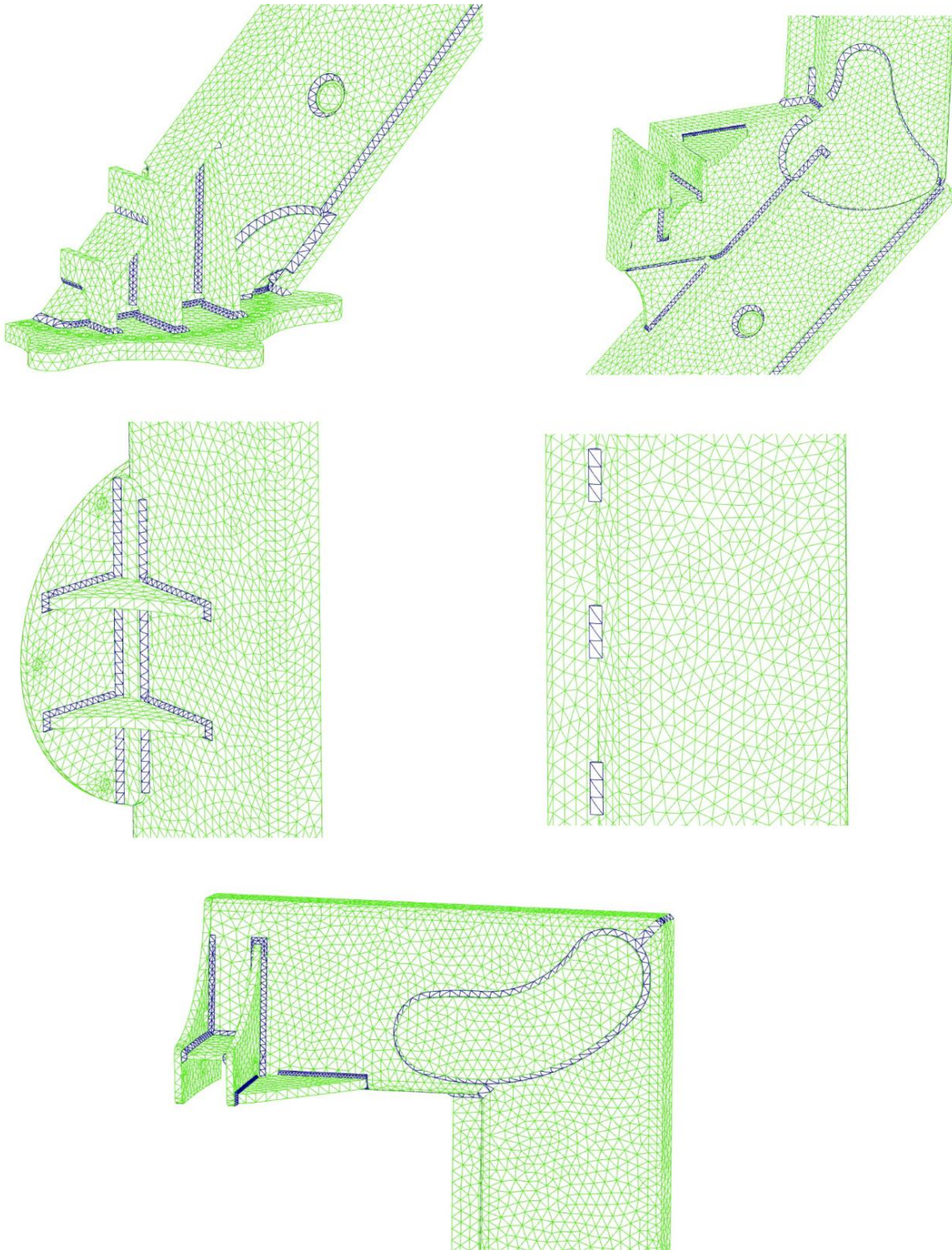


Fig. 4.17 Mesh Quality tool.

Details of the grid are presented in Fig. 4.18.



*Fig. 4.18 Mesh details. Green for mild steel parts and blue for welding material MC-50.*

# Chapter 5: Meta-analysis

According to the Standard we follow, IEC 61400-2:2013, the analysis applies to material properties evaluated at 95% probability with 95% confidence interval. This data comes from the material supplier. In addition, we should be aware of factors that affect the integrity of the structure throughout its life. Factors such as full-size structures, construction methods, fatigue and load spectrum, environmental effects, and geometric effects. These are required to classify our structure as 'Full Characterization'. Otherwise, we fall into the 'Minimal Characterization' category and must then select a higher safety factor, as shown in Table 6 of the Standard (Fig. 5.1).

**Table 6 – Partial safety factors for materials**

Material characterisation	Fatigue strength, $\gamma_m$	Ultimate strength, $\gamma_m$
Full characterisation	1.25 <sup>a</sup>	1.1
Minimal characterisation	10.0 <sup>b</sup>	3.0
<sup>a</sup> Factor is applied to the measured fatigue strength of the material.		
<sup>b</sup> Factor is applied to the measured ultimate strength of the material.		

*Fig. 5.1 Table 6 from chapter 7.8.1 in standard IEC 61400-2:2013.*

In recognition that we do not know enough about the full characterization of the design. A safety factor equal to 3 was chosen as the minimum target.

## 5.1 Case 1 Results - 18m/s

The results for the first case showed that the construction was far from adequate. The displacement is just exceeding the 5 mm and the maximum von Mises stress is 31.42 MPa, well below the yield strength.

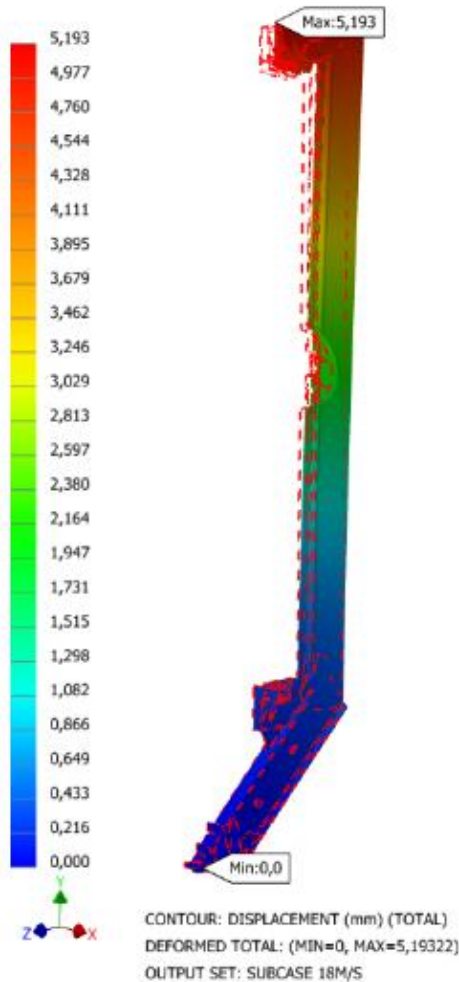


Fig. 5.2 Displacement for case 1.

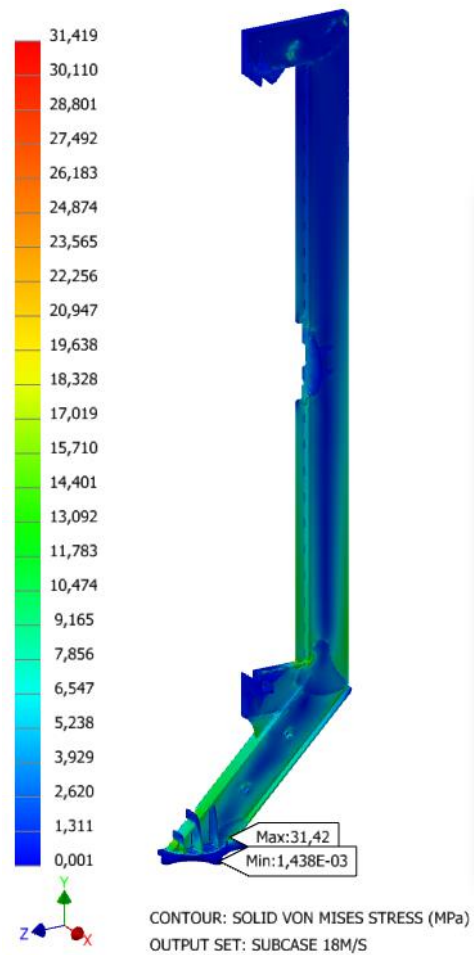


Fig. 5.3 Solid Von Mises stress for case 1.

The safety factor of 9.2 is more than three times the value required by the standard. A closer look at the isosurface of the safety factor shows that they occur mainly along the weld at the column reinforcing bars and some at the welds of the mounting flange stiffeners.

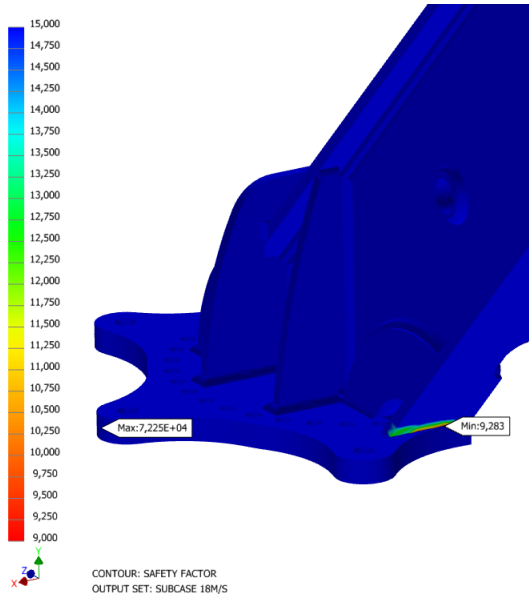


Fig. 5.4 Safety factor for case 1.

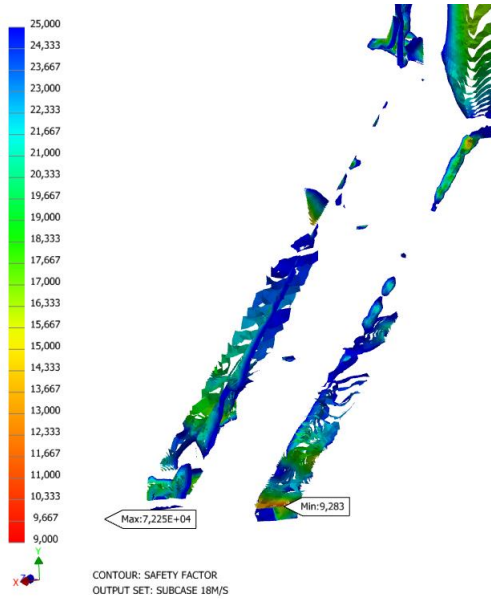


Fig. 5.5 Safety factor iso-surface for case 1.

## 5.2 Case 2 Results - 50m/s

The second case with extreme weather conditions is much more challenging. The displacement is not so far away, with the largest value being only 20 mm.

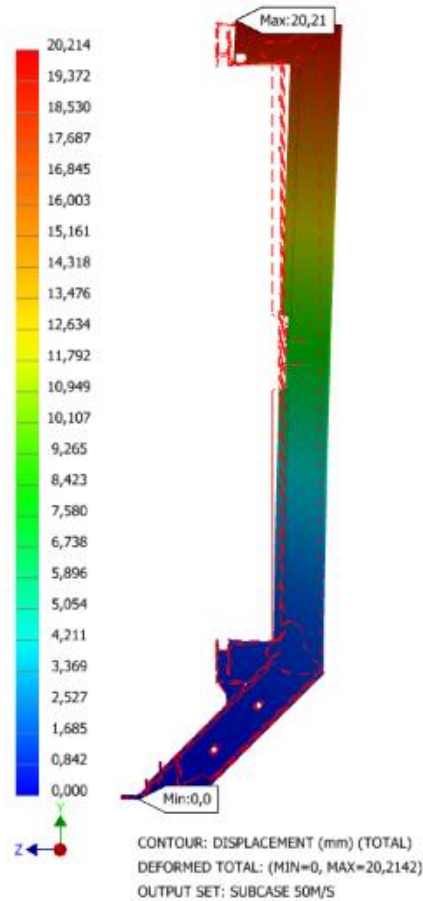


Fig. 5.6 Displacement for case 2.

The maximum von Mises stress is 103 MPa, which does not exceed the yield strength, but is quite high compared to the first case.

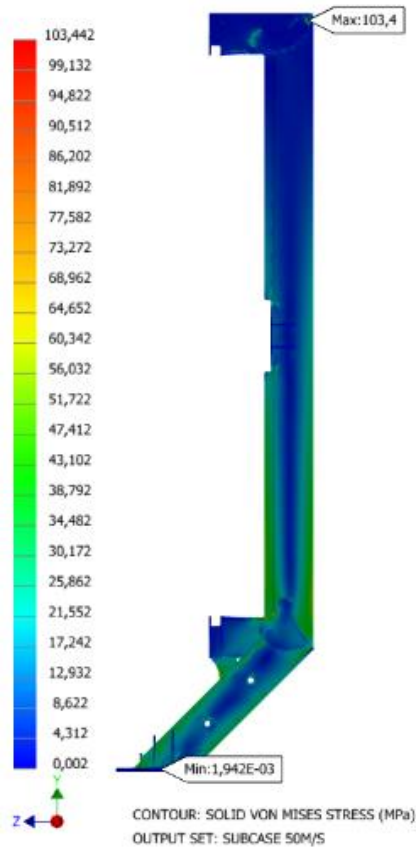


Fig. 5.7 von Mises stress for case 2.

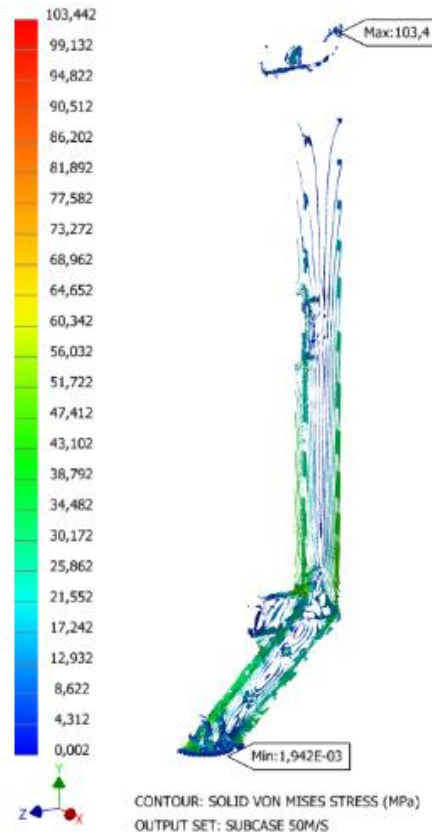


Fig. 5.8 von Mises Iso-surface for case 2.

As expected, the maximum von Mises stresses occur at the bottom of the column and along the weld of the column reinforcing plates. This is most clearly illustrated by the von Mises isocurves. Typically, the stresses are located on or near the welds. This is reasonable, because the other surfaces are "Separated" and can slip or detach to each other. Inevitably, the forces pass through the welds, which are defined as "Bonded" in the analysis.

The safety factor in this case has a value of 2.93, just below the threshold of '3'. The position of the minimum is (unsurprisingly) at the lower back of the column, where all compressive forces are concentrated. In the event that the turbine needs to be certified as 'Class I', further reinforcement of the structure is necessary.

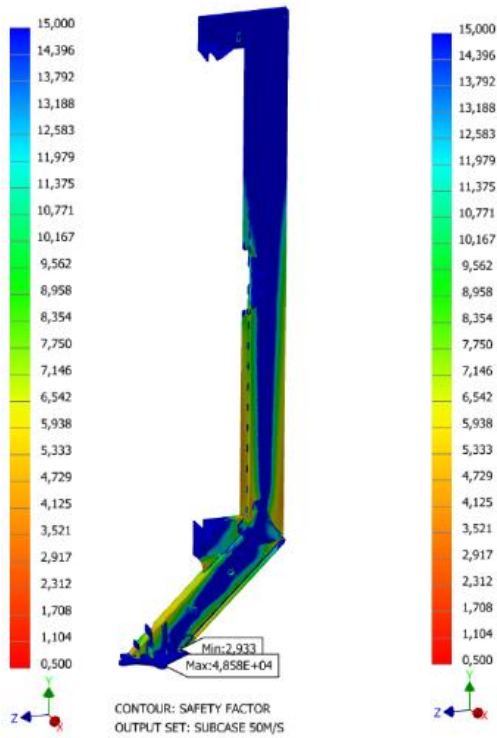


Fig. 5.9 Safety factor for case 2.

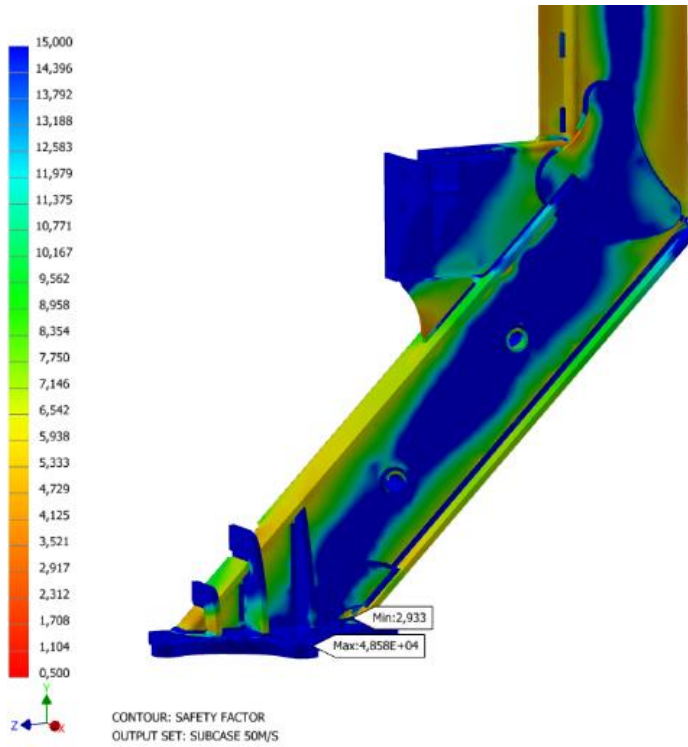


Fig. 5.10 Safety factor for case 2; detail 1.

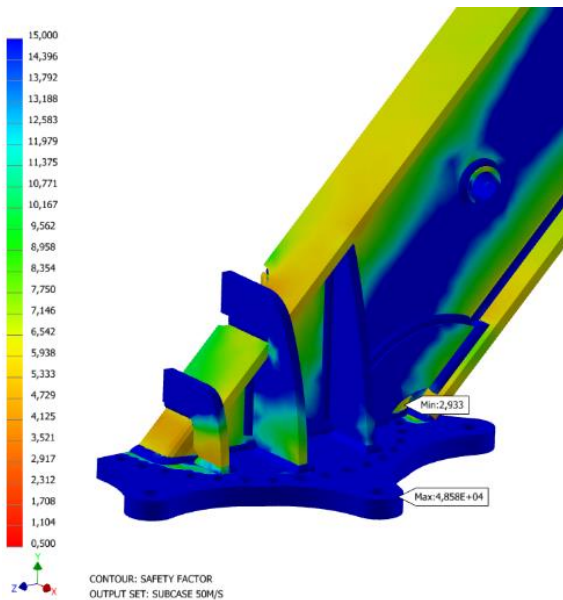


Fig. 5.11 Safety factor for case 2; detail 2.

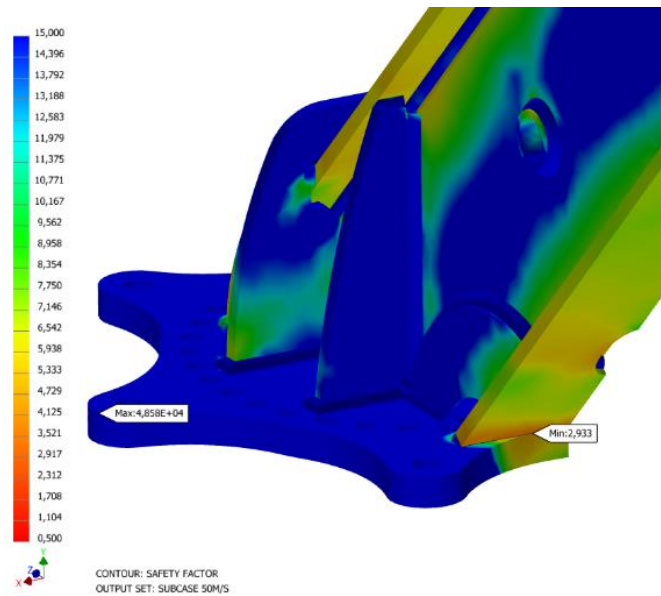


Fig. 5.12 Safety factor for case 2; detail 3.

### 5.3 Modal Analysis

Modal analysis is the simplest analysis and the important data gathered from this is what the "resonant frequencies" of geometry are. It is only important for structures that are subject to vibration, such as engine imbalance, earthquakes, or wind resonance (we have all three). It is not related to any loading at this stage, only to geometric dynamics.

The modal analysis gives as result the "natural frequencies", "mode shapes" and "mode participation factors". The maximum vibration occurs at the natural frequencies, which we generally try to minimize. So it tells us at what frequencies the system is susceptible to oscillation. If, after modal analysis, the natural frequencies are in the range of the excitation frequencies, we usually, but not always, try to modify the structure to shift the natural frequencies out of the range of the excitation frequencies. The mode shapes tell us how the structure deforms at certain natural frequencies.

The mode shapes tell us in which regions high stresses would occur if the deformed shape were similar to the mode shape. This is useful because we usually do not want high stresses to occur in the weld regions, as this can affect the fatigue life of the structure. The mode participation factors also tell us which modes would be most excited. The effective masses tell us which modes need to be considered for the given dynamic simulations (frequency response or transient dynamics) [Abbas, 2019].

Normal modes are better if they precede the bulking analysis to reveal the weak points of the geometry at different frequencies. Then, the designer must make the necessary reinforcements at the points most affected at the frequencies at which the structure operates.

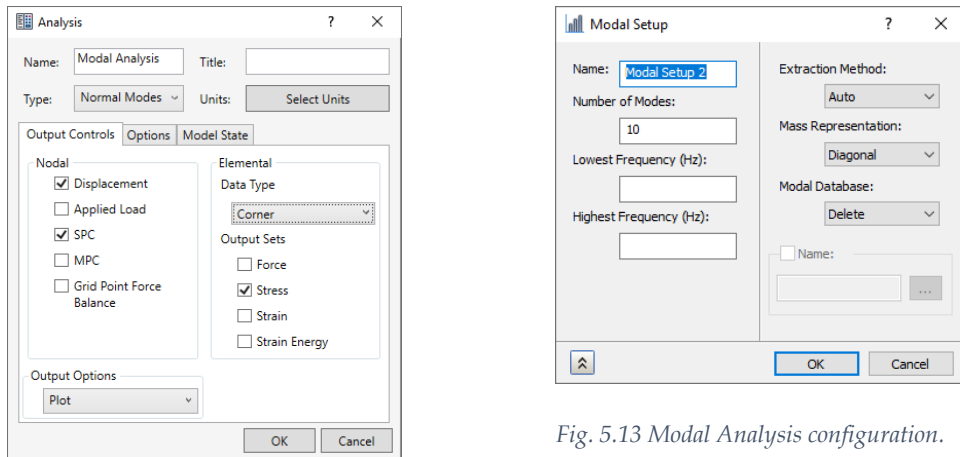


Fig. 5.13 Modal Analysis configuration.

We set up the analysis to determine the first 10 Modes. The modal modes are independent of the size of the loads.

## 5.4 Modal Analysis Results

The results of the analysis are presented in Fig. 5.14.

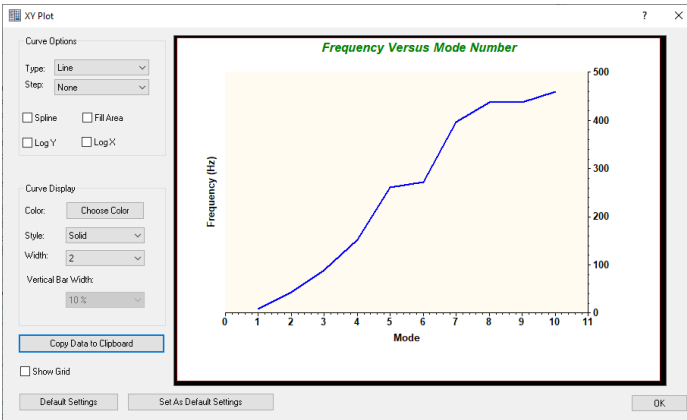


Fig. 5.14 Frequency versus Mode.

Mode	Frequency (Hz)
1	8,25925
2	42,6579
3	88,8716
4	151,475
5	261,376
6	271,916
7	396,556
8	436,856
9	437,221
10	458,828

The most interesting mode is the first. At the maximum operating speed, the rotor rotates at 300 rpm (5 Hz), while the maximum permissible speed is 600 rpm (10 Hz). So, the first mode is in the operating frequency range of the wind turbine, and this is undoubtedly a problem.

The other frequencies are much higher and are unlikely to be naturally induced. Seismic vibrations do not usually exceed 20 Hz, so even the second mode (42 Hz) is considered out of the frequencies of interest.

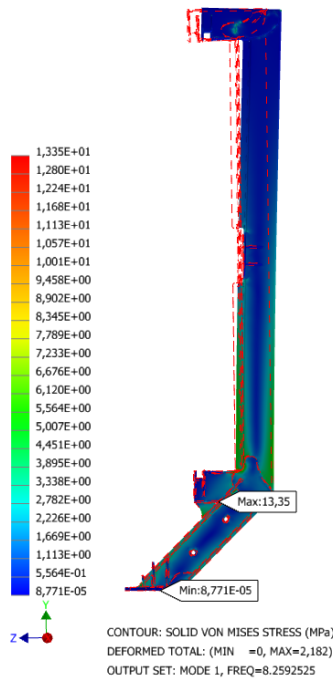


Fig. 5.15 Mode 1 Stress.

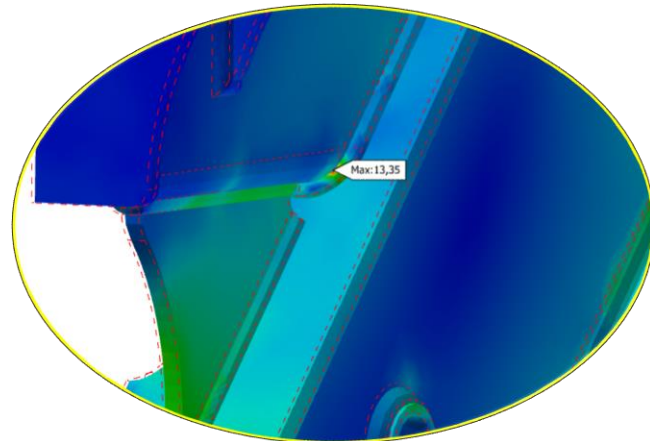


Fig. 5.16 Mode 1 Stress detail.

As mentioned earlier, the Modes Analysis does not depend on the loadings. Similarly, the results are not given in their actual scale and magnitude, but as factors of multiples of 1. Thus, the result shown in Fig. 5.16 with a maximum load of 13.35MPa means that at an oscillation frequency of 8.25Hz at this point, which previously had a load of 1MPa, now has 13 times the load. This is a very high coefficient indeed, but it depends on where the point is placed. Actually, this point at that place does not really pose a risk to the structure because it is not in a heavily loaded area.

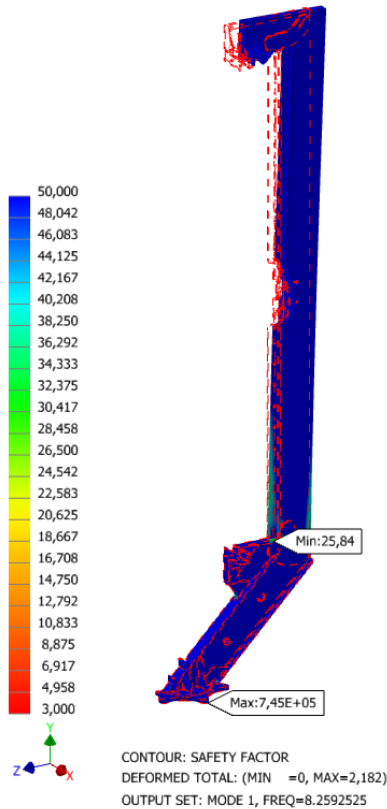


Fig. 5.17 Mode 1 Safety factor.

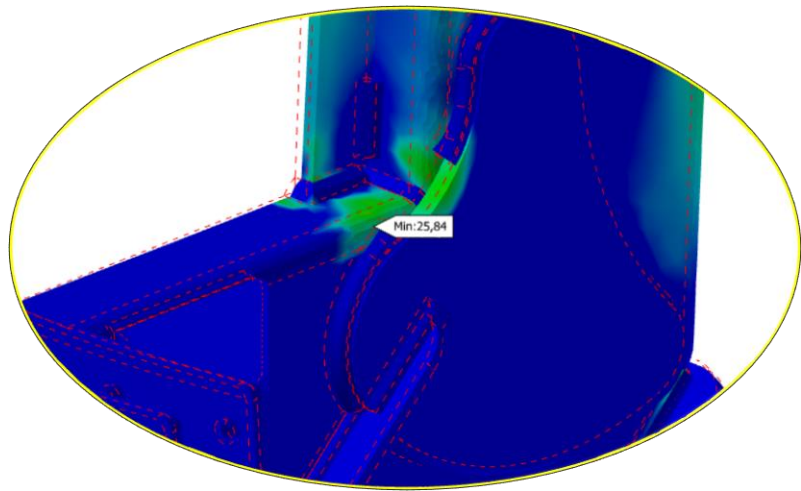


Fig. 5.18 Mode 1 Safety factor detail.

The safety factor is at least 25.84, indicating that the frequency of the first mode of oscillation, although lawfully induced at a certain point, fortunately has no undesirable effects on the structure.

The following modes can have very destructive effects, as can be clearly seen in Fig. 5.19. The advantage, however, is that they are beyond the frequencies we expect.

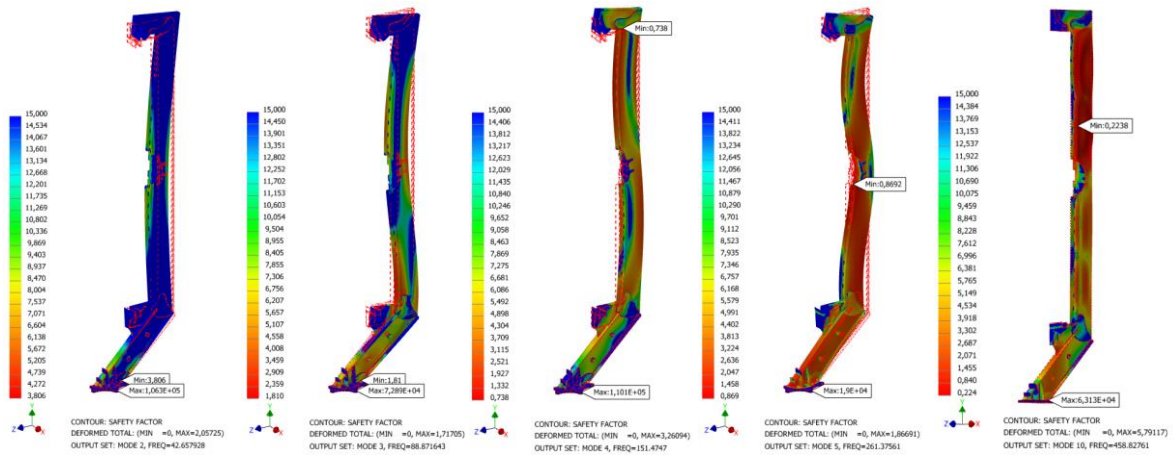


Fig. 5.19 Modes comparison.

## 5.5 Linear Buckling

The next analysis concerns buckling. Structures of high length and small cross-section, as in our case, are often destined to bend and suddenly buckle in a catastrophic way. It is one of the most popular types of analysis, because it is not difficult to perform. Another name for Linear Buckling Analysis is Eigenvalue buckling or Euler buckling analysis, as it is used to predict the theoretical buckling strength of an elastic structure.

A linear buckling analysis is similar to modal analysis in many ways. Both linear buckling analysis and modal analysis (which is also linear) can predict a large number of modes. In buckling analysis, only the first mode is of practical importance. This is because higher buckling modes have limited or virtually no chance of occurring.

The buckling mode depicts the shape the structure takes when it deforms in a particular mode, but gives no indication of the numerical values of displacements or stresses. These values can be displayed as usual, but they are only relative. In other words, they give qualitative information, but not about the actual magnitude of these features.

FEA software overestimate buckling load factors, because they must compensate for modeling errors and discretization errors. FE Models often have no imperfections, while loads and supports are applied perfectly with no misalignment. However, loads are always applied with misalignment, surfaces are not exactly straight, and columns are never completely rigid. In the real world, there will always be irregularities. Therefore, designers should interpret the results of linear buckling analysis with caution, because they must consider the combined effect of discretization errors (a small effect) and modeling errors (a large effect).

Linear buckling is useful:

Fast failure check: If linear buckling case gives minimal eigenvalue smaller than 1.0 your model will be unstable without a doubt! This is definitely the fastest way to verify such a case.

Imperfection shape: Shape obtained from LBA is often used as imperfection shape. This may not always be desirable, but often is sufficient (especially in beam models).

Model verification: You can quickly check if everything “works” in your model. You will see if it behaves as it should, deforms correctly etc.

Quick estimate: You can see which regions will have stability issues. You will also get an estimate on how close your model is to stability failure [Skotny, 2017].

### 5.5.1 Set-up

We create a new analysis with the type "Linear Buckling". The initial assumptions, such as semi-symmetry, material properties, mesh and constraints are as described for the linear static analysis. The difference is that this instance we only study the case of 50 m/s, which is clearly the worst case from the point of view of stress.

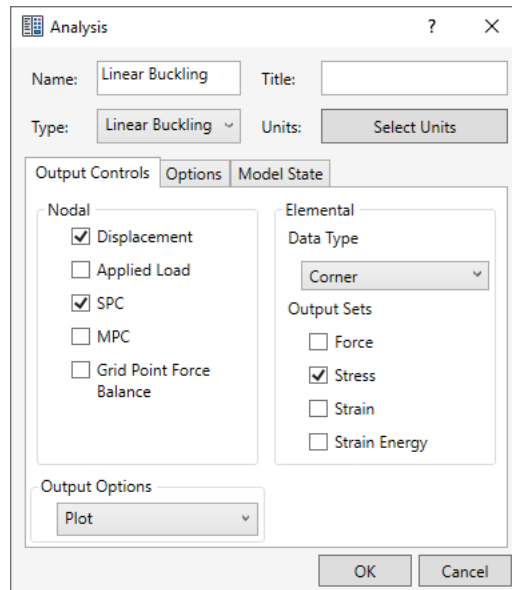


Fig. 5.20 Set up for Linear Buckling.

### 5.5.2 Linear Buckling Results

The Eigenvalue can also be referred to as a multiplier. This is the case because if you multiply the applied loads by this value, you achieved a load that causes the stability failure. For example, if we had a value of less than one, then it requires a load less than that which will cause problems, so we understand from the beginning that our structure needs more strengthening.

In our case, the value 141.30 given by the analysis (Fig. 5.21) is a very positive result. This is because we would need 140 times more load to trigger buckling in our system. Of course, this should not be reassuring because the Buckling method has fundamental limitations. One of them is that positive outcome is unreliable. Normally, the Eigenvalue should be greater than 1.0, but even then this does not mean that stability failure can be ruled out [Skotny, 2017].

As can be seen from the results, the buckling phenomenon occurs in the lower part of the second section of the column. The first part of the hollow beam is well reinforced with dual reinforcing plates above and below the hollow beam. We also added two reinforcing tubes in the middle of the same section to prevent buckling of the side walls, and this seems to work very well. So, the forces of the calculation immediately refocused toward the next section, which was identified as exposed without reinforcement.

We could reinforce this piece as well, but before we take any action, we should consider whether this is necessary. Here we would suggest carrying out a nonlinear analysis.

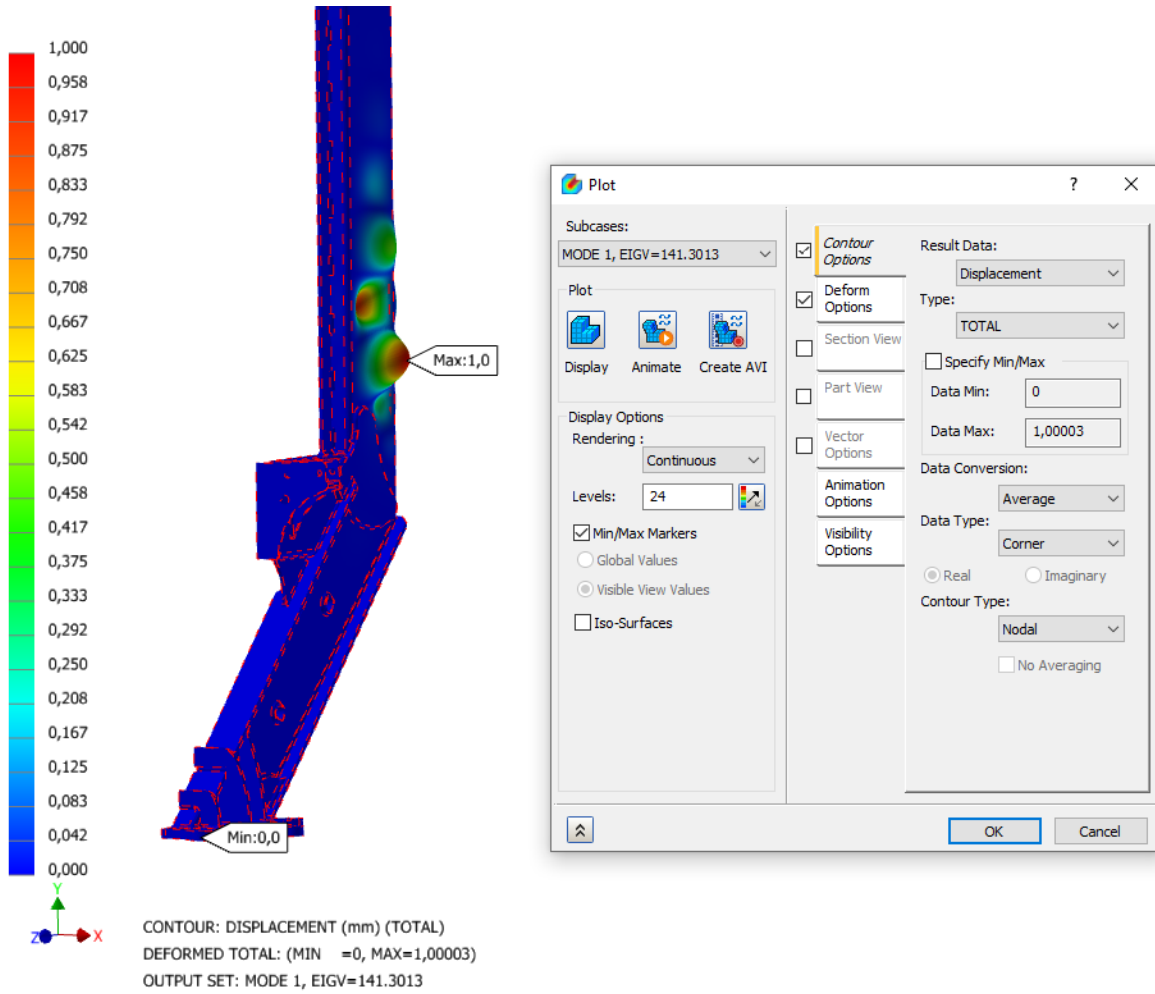


Fig. 5.21 Buckling Analysis Displacement.

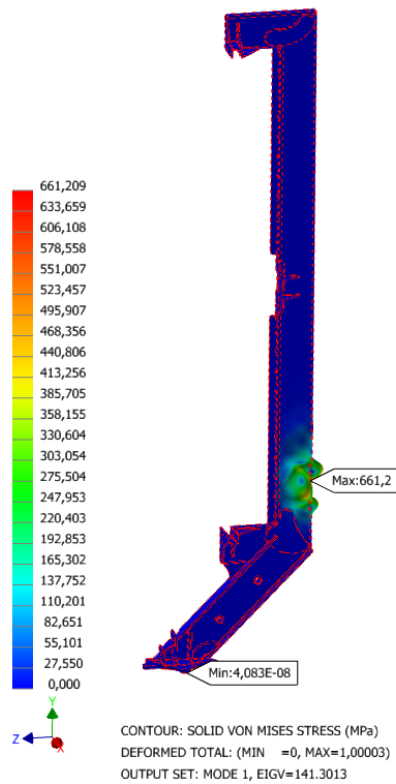


Fig. 5.22 Buckling Analysis Stress.

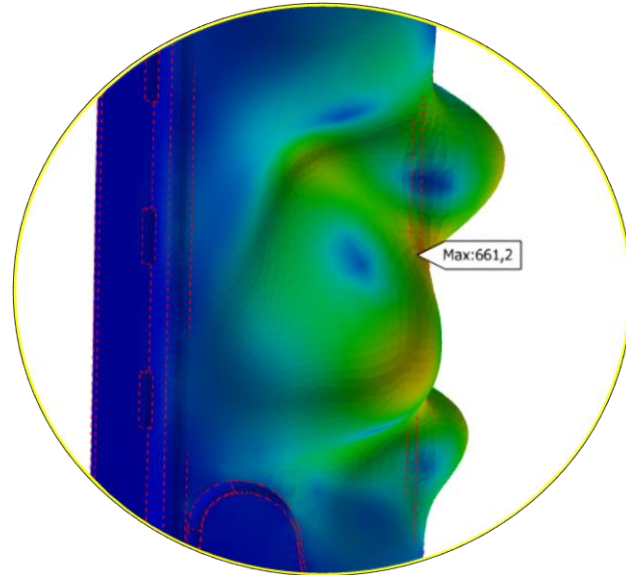


Fig. 5.23 Buckling Analysis Stress detail.

We can clearly see that the model is deforming. As we have already mentioned, this is not an actual deformation. By default, the maximum value of the displacement equals to 1.0. To get a different value, you need to normalize it differently. The shape displayed here shows where and in what form the stability failure will occur. This means that our structure must be further strengthened in this area to resist the buckling stresses. Possible solutions would be to weld reinforcing plates to the sides of the hollow beam or to create holes and weld tubes as in the first part of the hollow beam.

The Von Mises stresses at their maximum point is 661 MPa, which is approximately three times the yield strength. So, we would also expect a degree of safety close to 0.35, as is the case if we look at Fig. 5.25.

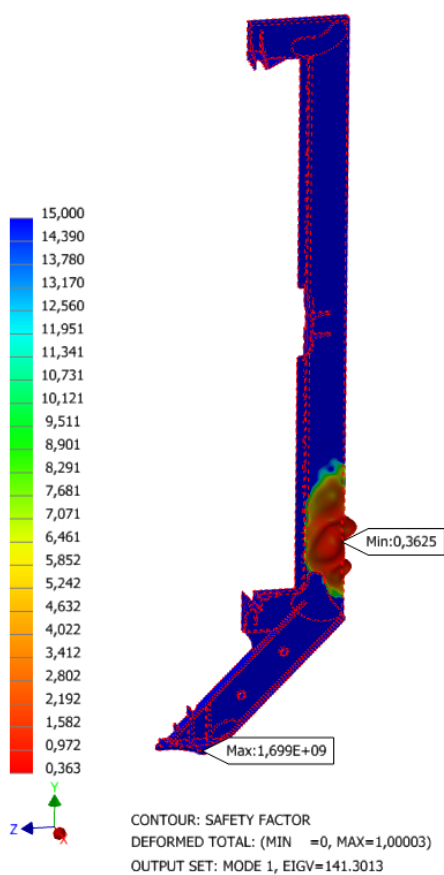


Fig. 5.24 Buckling Analysis Safety Factor.

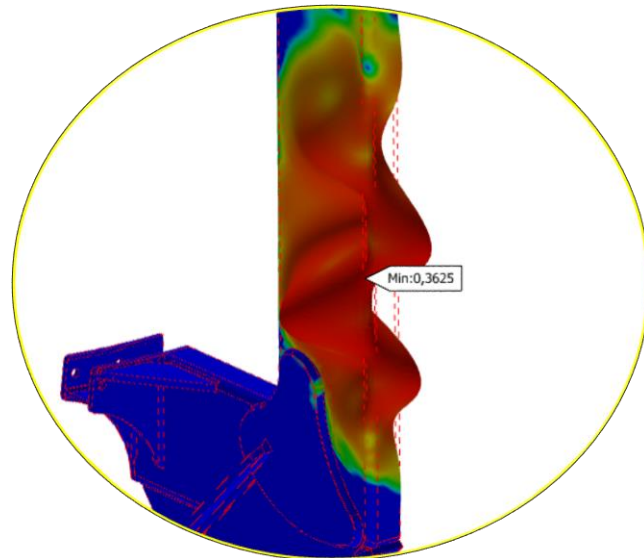


Fig. 5.25 Buckling Analysis Safety Factor detail.

### Buckling conclusions:

Obviously, our model does not seem to have stability problems with respect to buckling. But the linear buckling analysis does not show the aftereffect of buckling. It is not clear if the structure collapses or if it is no longer able to support loads in the buckled form. It is also not clear how much it will deform. To obtain more information, a nonlinear buckling analysis is required.

# Chapter 6: Conclusions

The results of this study can be summarized in two categories. The first category of conclusions concerns the way the simulations were modeled and conducted. Efforts were made to have the model represent as accurately as possible, a metal structure with all shapes and welds in their actual sizes and properties. This choice brought several benefits related to a better understanding of the model behavior by the designer. It was possible to determine exactly where the defects occurred and how the deformations appeared in the model. This made it possible to make continuous improvements to the model in details that are critical to the design of a correct metallic assembly. For example, the geometries of the metal reinforcements, the surfaces to be welded, and the welds themselves were specified. The result of this process was a detailed 3D visualization of a model containing precise instructions for the construction.

This method has some disadvantages that must also be pointed out:

- Both the modelling and the preparation of the analysis were time consuming.
- The analysis itself was also time-consuming to solve, with a correspondingly large computational load and demand on computing resources.
- Such detailed modelling often can lead to endless refinements. Local amplification of the model at one point often resulted in "pushing" the problem to a neighboring area, and so on.

The second category of conclusions concerns the results of the simulations. The forces resulting from the simulations of CFD proved to be significant in magnitude and intensity. Of course, the real forces in the actual model with the diffuser mounted will also be significant. This was to be expected since some of the improved performance is due to the resistance of the diffuser to the ambient air. This made the task of achieving a safety factor of more than 3 in the static model much more difficult.

The results are proven to be robust, since as many simulations with similar input data were repeated they produced similar results. The stability of the results can also be seen in the difficulty we had in improving the safety factor. Since the material mass and the basic geometry did not alter significantly, it was difficult to improve the safety factor at the given load magnitude.

In the vast majority of simulations, the results were consistent with the expectations of engineering logic. The stress concentration was at the expected locations, as were the deformations. Buckling was also exactly at the point where it could be predicted, so precautions were taken to reduce it. In cases where unreasonable indications were shown, it was an alarm signal that there was a gap in the configuration or an oversight during the setup.

Further analysis in the form of Non-Linear Static Analysis and Non-Linear Buckling Analysis may indicate further structural requirements. Both types of investigations are essential for a better understanding of the behavior of the structure. Moreover, they allow a better study of the structure when it is loaded beyond plastic deformation. At a later stage, a Fatigue Analysis can be performed to complete the study by determining the life of the structure.

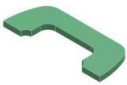
# Terminology

*Feathering:* Change the pitch angle to turn the blades parallel to the airflow to act as a brake for the rotor.

*Von Mises stress:* The Von Mises stress is a value used to determine whether a particular material will yield or break. It is mainly used for ductile materials, such as metals. The von Mises yield criterion states that if the von Mises stress of a material under load is equal to or greater than the yield strength of the same material under simple tension, then the material will fail. The von Mises yield criterion generally shows how far the principal stresses diverge from each other.

# Appendix A - Parts List

Item	Part Number	Thumbnail	Thickness	Mass	Material
1	Column Flange		40	140,991 kg	Steel, Mild
2	EN 10210-2 - 400 x 200 x 16 - 2078.89		16	248,276 kg	Steel, Mild
3	EN 10210-2 - 400 x 200 x 16 - 6182.84		12,5	824,948 kg	Steel, Mild
4	EN 10210-2 - 400 x 200 x 16 - 1000		12,5	106,347 kg	Steel, Mild
5	EN 10210-2 - 400 x 200 x 16 - 600		10	60,403 kg	Steel, Mild
6	DIN 1025 - IPE 220-800		10	20,082 kg	Steel, Mild
7	Reinforce Front		15	80,994 kg	Steel, Mild
8	Reinforce Back		15	165,608 lbmass	Steel, Mild

9	Column Stiff_A		20	5,564 kg	Steel, Mild
10	Column Stiff_B		20	14,490 kg	Steel, Mild
11	Column Stiff_C		20	5,769 kg	Steel, Mild
12	Ring Holder_O		10	5,123 kg	Steel, Mild
13	Ring Holder_B		15	12,917 kg	Steel, Mild
14	Ring Holder_F		15	19,310 kg	Steel, Mild
15	Ring Holder Stiff		15	4,284 kg	Steel, Mild
16	Hub Mount Flange		15	37,152 kg	Steel, Mild
17	Column Stiff_D3		15	21,344 kg	Steel, Mild

18	Hub Mount Stiff		15	2,750 kg	Steel, Mild
19	Hook		20	7,650 kg	Steel, Mild
20	Column Stiff_L		15	4,677 kg	Steel, Mild
21	Column Stiff_M		15	15,141 kg	Steel, Mild
22	ISO 1035/3 - 50 x 15 - 600		15	3,487 kg	Steel, Mild
23	Column Stiff_E		15	3,020 kg	Steel, Mild
24	ISO 1035/3 - 80 x 30 - 2400		30	44,981 kg	Steel, Mild
25	ISO 4019 - 76.1x6.3 - 335.03		6,3	3,221 kg	Steel, Mild
26	ISO 10799-2 - 76.1x6.3 - 230		6,3	2,494 kg	Steel, Mild

# Appendix B – CFD Data

Case 1 - NEC						Moment	
Ambient Velocity - Vo [m/s]	Density - ρ [kg/m <sup>3</sup> ]	Dynamic Viscosity - μ [Ns/m <sup>2</sup> ]	RPM	TSR		477	
18.0	1.200	0.000018	300	4.7141		643.95	Nm
						643950	Nmm
Diffuser - Drag [N]	Internal Flap - Drag [N]	Rotor Thrust [N]	Total Axial Force [N]		Half		
4582.47	1558.69	2679.35	8820.52			321975	
Safety factor 1.35	6186.34	2104.24	3617.12	11907.70			
	8290.58		Half	-5954		GRAVITY	
						-9806.65	mm/s <sup>2</sup>
Case 2 - EEC							
Ambient Velocity - Vo [m/s]	Density - ρ [kg/m <sup>3</sup> ]	Dynamic Viscosity - μ [Ns/m <sup>2</sup> ]	RPM	TSR			
50.0	1.2	0.000018	No rotor	-			
	Diffuser - Drag [N]	Internal Flap - Drag [N]	Rotor Thrust [N]	Total Axial Force [N]			
No conversion	-	-	0.00	0.00		0.00	
Pick values	24000	11550	0.00	35550			
+ Safety factor	32400	15593	0.00	47993			
			Half	-23996			
						-23996	
	68%	32%					

Case A.

# Appendix C – Welding Wire specification

## MC-50T

For mild steel and 50kgf/mm<sup>2</sup> class high tensile strength steel

AWS A5.18 ER70S-6  
KS D 7025 YGW12  
JIS Z3312 YGW12

### Applications

Butt and fillet MAG welding of structures such as automobiles, vehicles, electric appliances, ships, steel frames, bridges in all position.

### Characteristics

- (1) MC-50T is a solid wire whose arc stability is good at low current ranges (short-circuiting arc range) and spatter loss is low.
- (2) It is suitable for all-position welding of steel sheets by CO<sub>2</sub> or Ar+CO<sub>2</sub> mixed gas shielding, for higher speed welding.
- (3) The arc stability is good in wide range of current.

### Notes on Usage

- (1) Flow rate of shielding gas (CO<sub>2</sub>) should be 20ℓ/min generally.
- (2) Flow rate of shielding gas should be 25~30ℓ/min under the condition of 2m/sec wind speed and use wind screen under the condition of over 2m/sec wind speed.
- (3) Keep the distance between tip and basemetal within 10~20mm at less than 300A Welding current and within 20~25mm at over 300A.

### Typical chemical composition of weld metal (%)

(Shield Gas : 100%CO<sub>2</sub>)

C	Mn	Si	P	S
0.09	1.8	0.50	0.015	0.012

### Typical mechanical properties of weld metal

PWHT	YP N/mm <sup>2</sup> (kgf/mm <sup>2</sup> )	TS N/mm <sup>2</sup> (kgf/mm <sup>2</sup> )	EL %	IV J (kgf-m)		Shield gas
				0℃	-20℃	
As welded	470(48)	550(56.1)	30	120(12.2)	100(10.2)	100%CO <sub>2</sub>
As welded	540(55.1)	610(62.2)	28	140(14.3)	120(12.2)	80%Ar+20%CO <sub>2</sub>

### Size & recommended current range (DC+)

Dia. (mm)		0.9	1.0	1.2	1.4	1.6
Amp.	F	50-200	50-200	80-350	100-470	200-550
	H	50-140	50-140	50-160	100-180	-
	OH	50-120	50-120	50-140	-	-

• Approval : ABS, BV, DNV, GL, KR, LR, NK, CWB

# References

- (ISO), International Organization for Standardization. (2017). *ISO/TS 20273:2017 Guidelines on weld quality in relationship to fatigue strength*.
- (ISO), International Organization for Standardization. (2013). *Wind Turbines - Part 2: Small wind turbines (IEC 61400-2:2013)*.
- Abbas, Mir Aamir. 2019. Re: What is the usefulness of modal analysis?. [Online]. (2019). [https://www.researchgate.net/post/What\\_is\\_the\\_usefulness\\_of\\_modal\\_analysis/5d7a186ca5a2e2832d5ea364/citation/download](https://www.researchgate.net/post/What_is_the_usefulness_of_modal_analysis/5d7a186ca5a2e2832d5ea364/citation/download). .
- Chantharasenawong, Chawin, Jongpradist, Pattaramon and Laoharatchapruerk, Sasaraj. (2011). *Preliminary Design of 1.5-MW Modular Wind Turbine Tower*. Krabi, Thailand : The 2nd TSME International Conference on Mechanical Engineering, 2011.
- Dimopoulos, C. and Gantes, C. (2012). *Experimental investigation of buckling of wind turbine tower cylindrical shells with opening and stiffening under bending*. Athens, Greece : Thin-Walled Structures 54 (2012) 140-155.
- Georgios Mazanakis, Ioannis K. Nikolos. (2015). *INTERMEDIATE REPORT - 3 Verification of the new structure*.
- Georgios Mazanakis, Ioannis K. Nikolos. (2015). *INTERMEDIATE REPORT - 6 Non-linear simulation of the new structure*.
- H. Patel, S. Ramani. (2017). *FINITE ELEMENT ANALYSIS OF MONOPOLE TOWER FOR DOMESTIC WIND TURBINE*. Ahmedabad, India : JETIR (ISSN-2349-5162),
- Help, Autodesk. 2021. [Online] (2021). <https://knowledge.autodesk.com/support/inventor-nastran/learn-explore/caas/CloudHelp/cloudhelp/2021/ENU/NINCAD-ExplicitRef/files/GUID-187636CA-F2ED-4D08-A4BF-8EC6C9766732-htm.html>.
- Hu, Y., Baniotopoulos, C. and Yang, J. (2014). *Effect of internal stiffening rings and wall thickness on the structural response of steel wind turbine towers*. Birmingham, UK : Engineering Structures 81, 148-161.
- Huskey, A. and Prascher, D. (2004). *Tower Design Load Verification on a 1-kW Wind Turbine*. Reno, Nevada : National Renewable Energy Laboratory, NREL/CP-500-37112.
- Kaoshan, et al. (2017). *Nonlinear response history analysis and collapse mode study of a wind turbine tower subjected to tropical cyclonic winds*. London, UK : Wind and Structures, 25(1), pp. 79-100. doi: 10.12989/was.2017.25.1.079.
- Kurowski, Paul M. (2011). MachineDesign. [Online] 2011. <https://www.machinedesign.com/3d-printing-cad/fea-and-simulation/article/21831716/buckling-analysis-with-fea>.

- Lavassas, I., et al. (2003). *Analysis and design of the prototype of a steel 1-MW wind turbine tower*. Thessaloniki, Greece : Engineering Structures 25 (2003) 1097–1106, 2003.
- Lingaiah, K. (2006). *“Machine design data hand book” Volume-1, Fourth edition*. s.l. : Suma publishers, ISBN-131234567142681, 2006.
- Nikolos, Dr. Ioannis K. (2015). *INTERMEDIATE REPORT - 1 Numerical Estimation of Diffuser’s Drag*. 2015.
- Risø DTU National Laboratory for Sustainable Energy. (2002). *Guidelines for Design of Wind Turbines*. 2. Copenhagen, Denmark : DNV/Risø, 2002.
- Skotny, Lukasz. Enterfea. [Online] (2017). <https://enterfea.com/linear-buckling-explained/>.
- Stavros Leloudas, Ioannis K. Nikolos. (2016). *INTERMEDIATE REPORT - 9 Rotor-generator matching*.
- Stavros N. Leloudas, Ioannis K. Nikolos. (2016). *INTERMEDIATE REPORT - 11 Diffuser side loading & DAWT Load curves*.
- Stavros N. Leloudas, Ioannis K. Nikolos. (2016). *INTERMEDIATE REPORT - 2 A Literature Review on the Diffuser Augmented Wind Turbine Concept*.
- Tran, Anh Tuan, et al. (2015). *Buckling observation of door openings for wind turbine towers*. Tampere, Finland : Nordic Steel Construction Conference.
- Umesh, K., Bharath, P. and Mohamed, I. (2016). *Design and analysis of 2-MW wind turbine tower*. Karnataka, India : International Journal of Mechanical And Production Engineering, ISSN: 2320-2092, Volume- 4, Issue-10.
- Wang, L., et al. (2016). *Structural optimisation of wind turbine towers based on finite element analysis and genetic algorithm*. Cranfield, UK : Wind Energ. Sci. Discuss., doi:10.5194/wes-2016-41.
- Νικόλαος Τσουρβελοῦδης, Ιωάννης Νικολός. (2014). *Τεχνολογίες Παραγωγής*. Χανιά : Εκδόσεις Πολυτεχνείου Κρήτης. ISBN 978-618-81537-0-7.